CHALMERS

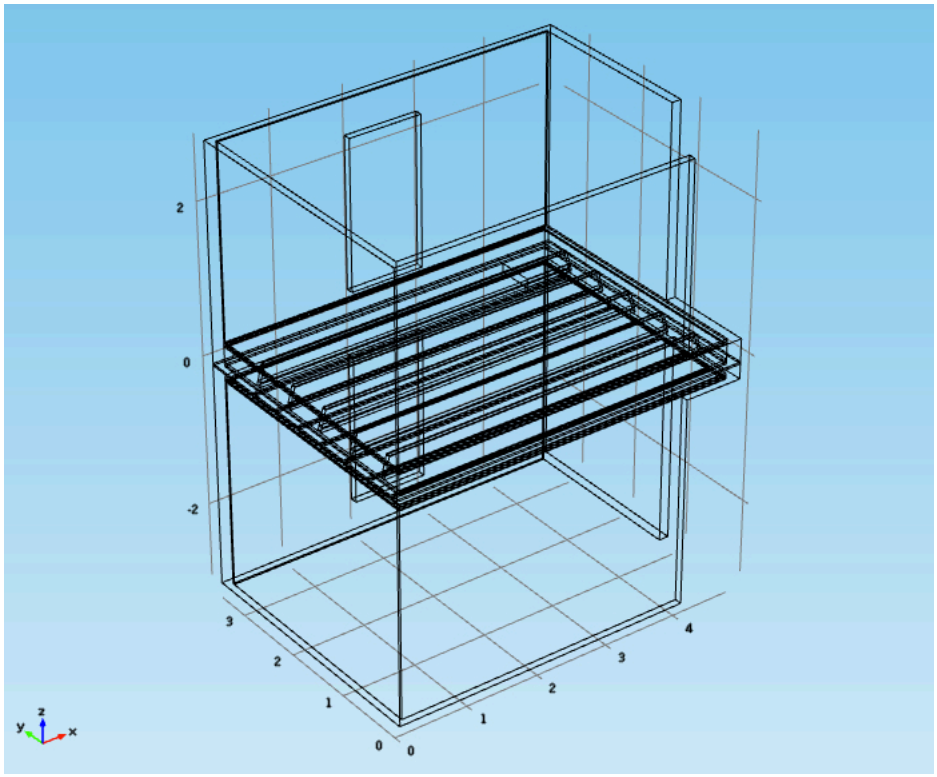

Finite Element Modeling for Cross Laminated Timber Constructions

Master's Thesis in the Master's programme in Sound and Vibration

NIKOLAOS-GEORGIOS VARDAXIS

Department of Civil and Environmental Engineering
Division of Applied Acoustics
Vibroacoustics or Room Acoustics Group
CHALMERS UNIVERSITY OF TECHNOLOGY
Göteborg, Sweden 2014
Master's Thesis 2014:153

MASTER'S THESIS 2014:153

Finite Element Modelling for Cross Laminated Timber Constructions

NIKOLAOS-GEORGIOS VARDAXIS

Department of Civil and Environmental Engineering
Division of Applied Acoustics
Vibroacoustics Group
CHALMERS UNIVERSITY OF TECHNOLOGY
Göteborg, Sweden 2014

Finite Element Modelling for Cross Laminated Timber Constructions

Master's Thesis 2014:153

Department of Civil and Environmental Engineering
Division of Applied Acoustics
Vibroacoustics Group
Chalmers University of Technology
SE-41296 Göteborg
Sweden

Tel. +46-(0)31 772 1000

Reproservice / Department of Civil and Environmental Engineering
Göteborg, Sweden 2014

Finite Element Modelling for Cross Laminated Timber Constructions
Master's Thesis in the Master's programme in Sound and Vibration
NIKOLAOS-GEORGIOS VARDAXIS
Department of Civil and Environmental Engineering
Division of Applied Acoustics
Vibroacoustics Group
Chalmers University of Technology

Abstract

This thesis is linked to an initial part of the research project Silent Timber Build, focused on a certain type of C.L.T. (Cross Laminated Timber) construction, a residential building in Fristad, Sweden. The objective is to study impact noise transmission, at the lower frequency range (10-200 Hz), where wooden dwellings perform inefficiently, in terms of acoustic quality. The vibrational behavior of lightweight structures and specifically a multilayered floor separating two vertically adjacent bedrooms are investigated. The test floor includes sound insulation and vibration isolation layers.

A numerical model of the test structure, the multilayered plate, is developed based on the Finite Element Method (F.E.M.), using COMSOL Multiphysics. The design process, the analysis and improvement of the calculated outcome concerning accuracy and complexity are of interest. In situ vibration measurements are also performed to evaluate the structures dynamic behavior in reality and consequently the validity of the modelled results.

The whole process from design to evaluation is discussed thoroughly. The uncertainties of the complex F.E.M. model and the approximations of the real structure are stated and analyzed. Numerical comparisons are presented including mechanical mobility and impact noise transmission results. The overall aim is to set up a template of calculations that can be used as a prediction tool and in the future by the industry and researchers. Improvement suggestions are made as well.

Keywords: Cross Laminated Timber, Vibration, Mobility, Impact Sound

Contents

Abstract iii

Contents iv

Acknowledgements vii

1. Introduction 1
- 1.1. Background . . . 1
- 1.2. Objectives . . . 1
- 1.3. Lightweight Structures and Cross Laminated Timber . . . 2
- 1.4. The Study Case . . . 3

2. Theory 7
- 2.1. Introduction to sound and vibration . . . 7
- 2.2. Motion of a Single-Degree-of-Freedom system . . . 7
- 2.3. Eigenfrequencies . . . 9
- 2.4. Damping . . . 9
- 2.5. Modal Analysis . . . 10
- 2.6. Waves in solids . . . 13
- 2.7. Material Properties . . . 14
- 2.8. The Finite Element Method . . . 15
- 2.9. Sound Radiation . . . 17

3. Implementation 19
- 3.1. Measurement of the Test Floor . . . 19
- 3.2. The F.E.M. Model Setup . . . 22
- 3.3. Impact sound levels approximation . . . 26

4. Results and Data 31
- 4.1. Measurements of the test construction Mobility graphs in narrow band 10-2000 Hz . . . 31
- 4.2. Comparison graphs; Measured and simulated mobility levels and impact noise levels by F.E.M. . . . 37

5. Discussion **47**
5.1. Analysis of the measured results 47
5.2. Comparison between F.E.M. results and measurements; mobility and impact noise levels 48
5.3. F.E. model evaluation and limitations 49

6. Conclusions **51**

7. Future work suggestions **53**

Bibliography **55**

A. Appendix **57**

Acknowledgements

The present M.Sc. thesis, conducted from January to September 2014, was an exciting, educating and invaluable experience for myself.

I would like to thank all the people from WSP Group, which offered me this interesting subject and the opportunity to get involved in a real industry project alongside my academic work. Special thanks goes to Klas Hagberg, as my industry supervisor for his unlimited support, Andreas Collebring and Jessica Fromell for their priceless help.

Deep gratitude goes to Jens Forssén, for supervising and supporting me through this thesis project, for all the effort, the encouragement, the indispensable guidance and his personal insight.

The completion of this project signifies also the end of my studies in Chalmers, Gothenburg. Therefore, I need to thank everybody in the division of Applied Acoustics, all the employees assisting in our education and especially professor Wolfgang Kropp, the head of department, for being a mentor and an inspiring persona.

Thank you, my fellow students, for the past two years we spent together. They might have been sometimes hard but in retrospect they were definitely fun, fruitful and full of unforgettable experiences. I wish you all the best in your future.

Last but not least, I owe a huge "thank you" to my family, parents and sister, for their unconditional support and understanding so far, for providing everything I need, during my lifetime and especially for the last years of studying abroad.

1. Introduction

1.1. Background

The demand for wooden buildings has been increased during the last decades due to their advantages compared to conventional heavy constructions. Specifically, in 1994 the Swedish regulations concerning timber housing prohibition, because of fire danger, were modified to comply with the European regulations. Some research projects took place in Europe, which concerned the investigation of multistorey lightweight dwellings in terms of acoustic comfort. Universities, research centers and industry consultancies were included in the consortia of research partners. The main focus was on the low frequency range, 20-200 Hz, where most of the noise problems occur in wooden structures.

Impact noise generation coming from walking, children playing or jumping, operating machinery (e.g. vacuum cleaner or a hammer) can lead to creating vibrations, which transmit sounds to neighboring rooms. Those types of nuisance can be a cause of complaint for the tenants and indicators of poor acoustic behavior for the whole construction [1],[2],[3].

Some of the above mentioned research programs of the last five years are Akulite and Acuwood [4], and this study is based on their outcomes as well [5]. The test object of this thesis is a floor structure from a timber building in Fristad, Sweden, the design of which is part of the ongoing research program Silent Timber Build [6]. The cooperating partners are Fristads Bygg [7], as the construction company, WSP Environmental Group [8], as the acoustic consultancy and KLH [9], the manufacturer of the CLT (Cross Laminated Timber) material.

1.2. Objectives

This thesis comprises a study of the vibrational behavior of lightweight structures and specifically a multilayered slab separating two vertically adjacent rooms. The floor under study includes sound insulation and vibration isolation layers and it is part of a complex structural joint.

A numerical model of the test structure, the slab, is developed based on the Finite Element Method, using a commercial scientific software package, COMSOL Multiphysics 4.3b [10]. The analysis and optimization of the calculated outcome in terms of accuracy, complexity and computation time is of major significance. In situ measurements were also performed to evaluate the structure's dynamic behavior in reality and consequently validate the modeled results.

The overall aim is to set up a process of calculations that can be used as a prediction tool in the future by the industry. For this reason, accurately optimized solutions are desired within the design process, without the need for expensive laboratory testing of structural samples.

1.3. Lightweight Structures and Cross Laminated Timber

The basic characteristics that make lightweight timber structures popular are; lower prices of construction materials, lighter structures, sustainable design, energy efficiency, lower carbon dioxide emissions, good behavior in fire incidents and integration with contemporary architecture and engineering.

Wood can be renewable, especially for the case of Scandinavian forests, therefore it is ecologically better compared to concrete. It is also significantly lighter in weight but also tolerant to stresses after being processed. Wood's properties related to thermal insulation are sufficient without any demand for excessive thickness of the timber walls. Additionally, it is a carbon dioxide storing natural material and after the proper industrial processing can be effectively fire protected [1],[2].

There are several types of engineered timber for building constructions in the market, such as Plywood, Timber Boards, Chipboards (made of small timber particles), Glued Laminated Timber or Cross Laminated Timber (CLT). The latter consists of spruce or pine strips glued and pressured with high power to form solid timber elements. The grains of the individual parts are placed crosswise, i.e. vertically to each other, before the gluing process to achieve high static behavior in every possible direction of dynamic stress, as presented in Figure 1.1 [9].

In practice, lightweight constructions are easier to build since a high level of prefabrication can be achieved. Individual parts, such as walls and floors, can be designed with precision in numerous forms and shapes. They can be produced in a manufactory, then transferred to the construction site and finally assembled together. The overall building process is faster and more sustainable because the environmental impact, regarding en-

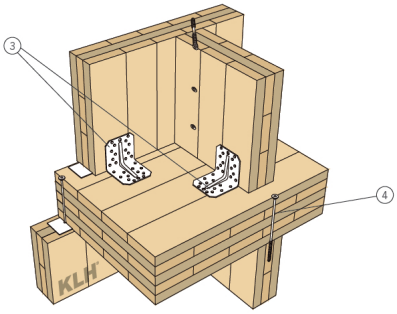

Figure 1.1.: Example sketch of Cross Laminated Timber elements by KLH [9]. Labels 3 and 4 refer to the metal connectors and bolts of the assembled structure.

Figure 1.2.: Photo of a house construction with CLT [9].

ergy consumption and pollution, is significantly smaller than for heavy constructions. There is also less dependence on external factors while erecting a CLT building, like the weather conditions for example [1],[2]. An example of a dwelling with a CLT structure is shown in Figure 1.2.

Besides all the construction advantages of timber, the acoustic conditions are not perfect in those structures, especially regarding low frequency noise transmission from adjacent rooms or apartments through walls and floors. Therefore, problems of acoustic and vibrational behavior have to be studied further and calculation tools for engineers need to be established.

1.4. The Study Case

As mentioned before in this report, the study case of this thesis is the acoustic evaluation of a multilayered floor. The test object is part of an actual residential timber

Figure 1.3.: Photorealistic view of the lightweight building under study, in Asbovagen, Fristad, Sweden. Designed by Tengbom Architects [7].

building which is presented in Figure 1.3. CLT is the main construction material of the dwelling and a three-dimensional construction plan of the whole structure, including only the CLT elements assembled together, is illustrated in Figure 1.4.

Regarding the details of the multilayered floor under investigation, a structural section is presented in Figure 1.5. The materials included in the slab, and therefore in the F.E. model developed, are the following with descending order starting from the top floor layer;
- light concrete screed,
- chipboard,
- mineral wool for sound isolation,
- elastomer for vibration isolation (Sylomer) which is on top of
- wooden beams,
- a layer of ballast to add mass to the structure,
- a main solid CLT plate to connect with the floorbeams and the supporting CLT walls as well,
- a suspended ceiling including mineral wool and a metal grid for connection and
- gypsum board for the ceiling layer.

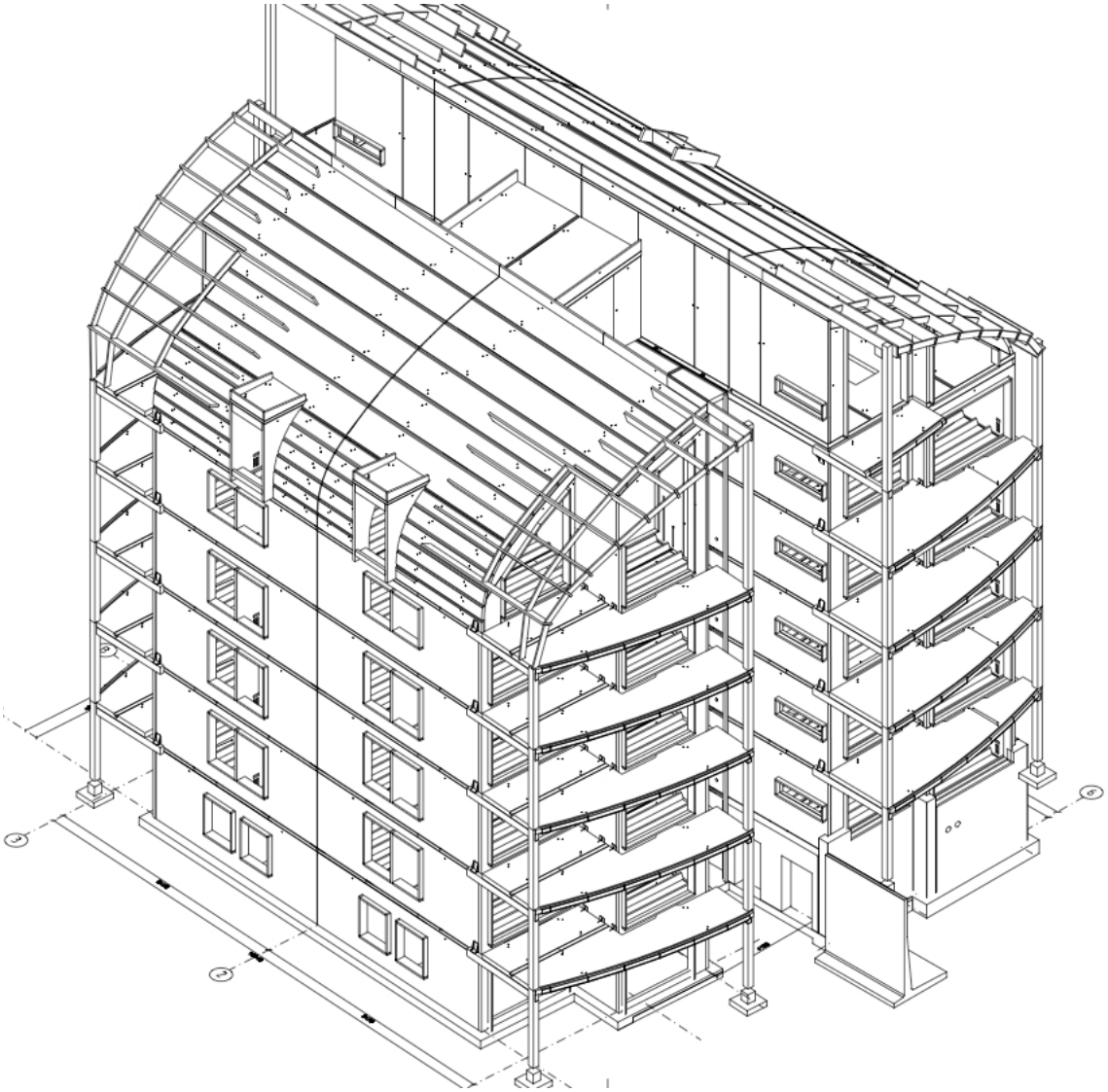

Figure 1.4.: Isometric view of the whole construction, showing only the CLT elements assembled and the concrete parts of the basement and the buildings' foundations. Picture by FristadsBygg [7].

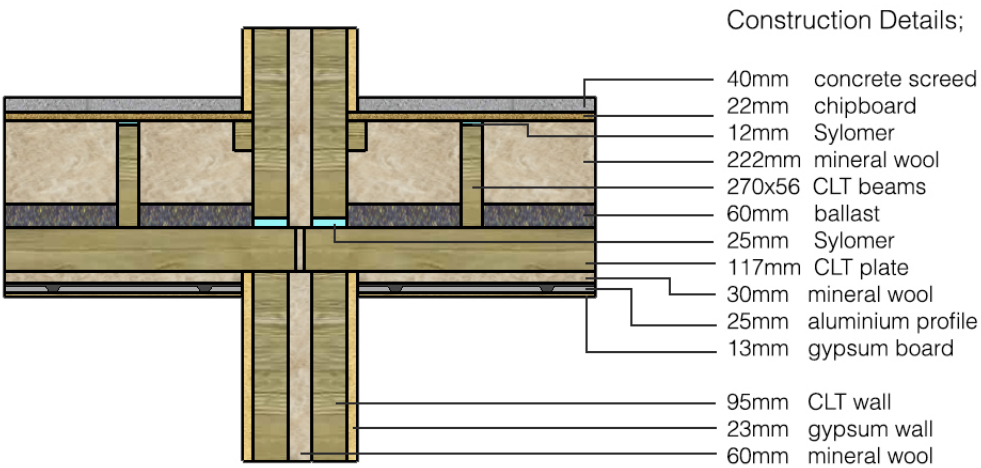

Figure 1.5.: Structural section showing the materials included in a junction of 4 adjacent apartments of the test building. Picture based on construction plans of FristadsBygg [7].

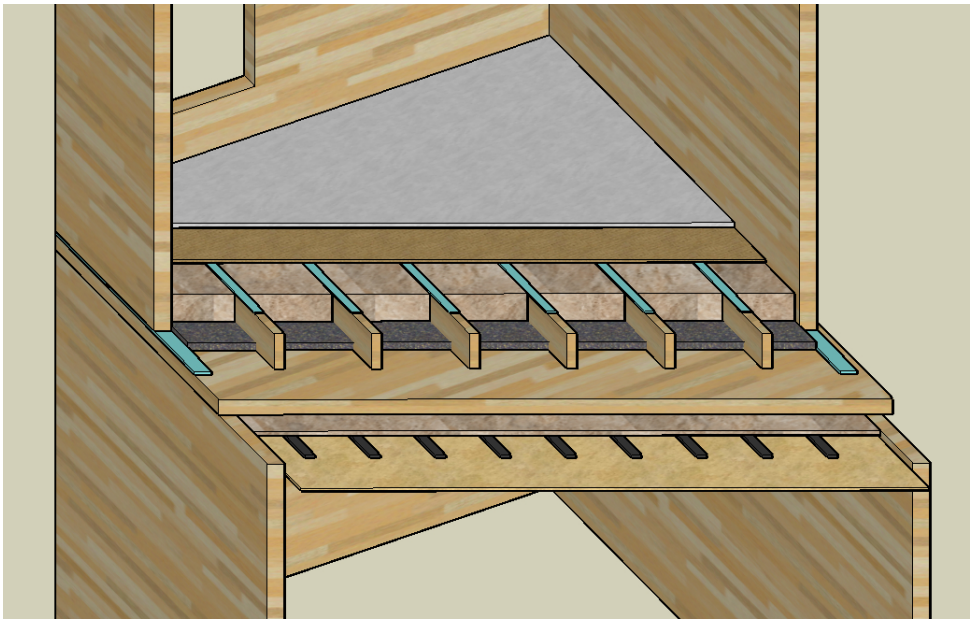

Figure 1.6.: Isometric structural section showing the material layers included in a junction of 2 vertically adjacent bedrooms of the test building. Other adjacent rooms or construction parts have been excluded from this sketch. The F.E. model developed in this study follows exactly the same design concept. Picture based on construction plans of FristadsBygg [7].

2. Theory

2.1. Introduction to sound and vibration

Sound and vibrations are interconnected by their physical and literal definition. The term vibration refers to the oscillatory motion around an equilibrium, i.e. a resting position, which takes place in a medium (air, gas or solid) with certain elastic properties. That oscillation could be periodic (e.g. a pendulum) or random like footsteps on the floor [11]. The physical meaning of sound is the propagation of waves created by mechanical vibrations in any elastic media. However, sound is also used to describe the sense of hearing as long as the stimuli that excite our ears are no more than propagating waves related to pressure changes in the surrounding air [12].

Initial properties of oscillations, used in sound and vibration, are the period T which is the time in seconds needed for one oscillatory cycle to be completed, the frequency f which equals $1/T$ and the angular frequency ω=$2\pi f$. Both f and ω have their units in Hz ($1/s$), named after Hertz [11].

To examine vibrations in building acoustics, certain parts of the structural dynamics theory need to be deployed, such as the motion equations. The vibrational strength is of interest and the appropriate quantity for its evaluation is the displacement of a mass or a point from its static equilibrium. The displacement $\vec{\xi}$ is a vectorial quantity, which means that it includes a magnitude and its direction in the Cartesian coordinates x, y, z. The first time derivative of displacement, $\delta\xi\ /\delta t$ or $\dot{\xi}$, is the velocity v and the second time derivative, $\delta^2\xi\ /\delta t^2$ or $\ddot{\xi}$, is the acceleration a. Those time derivatives are also vectorial and they may be used instead of displacement in vibrational studies.

2.2. Motion of a Single-Degree-of-Freedom system

The simplest case of mechanical vibration, which includes all the essential properties, is a single-degree-of-freedom system, denoted also as SDoF from now on. This means that it has only a single dynamic quantity under study, which is the displacement in the vertical axis z. The term ′degrees of freedom′ refers to the linear or rotational motions of a certain mass with respect to the x,y,z axes [13],[14]. A SDoF can consist of a mass,

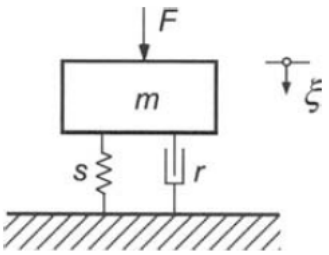

Figure 2.1.: A single degree-of-freedom system under excitation [13].

a spring and a damper, as illustrated in Figure 2.1, therefore it comprises a convenient model for representing dynamic systems in vibrational analyses.

In this case, a force balance gives the following intial equation of motion;

$$m\ddot{\xi}(t) + r\dot{\xi}(t) + s\xi(t) \quad = \quad F_0(t), \tag{2.1}$$

where m stands for the mass, r for viscous damping, s for spring stiffness and F_0 for the excitation force. The first term of that relation constitutes Newton's second law, according to which the total vector force ΣF to set an object in motion equals the product of the mass multiplied by the acceleration needed to move that mass. The second term is derived by Hooke's law of elasticity, which states that the force required for the deformation of a spring equals the displacement multiplied by its stiffness.

With a derivation in the time domain (according to the Fourier Transform it can be done by multiplying with $j\omega$) equation 2.1 can be written as;

$$-m\omega^2\xi(t) + rj\omega\xi(t) + s\xi(t) \quad = \quad F_0(t). \tag{2.2}$$

Assuming the system under examination is linear, the displacement for an excitation by more than one force can be calculated by a superposing (adding up) their responses. Although dynamic systems in reality might not be always linear, this approximation is generally safe. Therefore, a harmonic force excitation (one single frequency) of the form;

$$F_0(t) = F_0(\omega)e^{(j\omega t)}, \tag{2.3}$$

would lead to a harmonic displacement of the form;

$$\xi(t) = \xi(\omega)e^{(j\omega t)}. \tag{2.4}$$

Then a combination of all the above relations could lead to the expression;

$$-m\omega^2\xi(\omega)e^{(j\omega t)} + rj\omega\xi(\omega)e^{(j\omega t)} + s\xi(\omega)e^{(j\omega t)} \quad = \quad F_0(\omega)e^{(j\omega t)}. \tag{2.5}$$

which could be simply formulated for the frequency domain as;

$$\frac{\xi(\omega)}{F(\omega)} = \frac{1}{-\omega^2 m + rj\omega + s}. \tag{2.6}$$

The last numerical expresion is a so called Frequency Response Function (FRF), which corresponds to the displacement response of the system under excitation by force at each frequency component. This response is called Receptance. Equation 2.6 could also be written with the velocity term instead of displacement such as;

$$\frac{v(\omega)}{F(\omega)} = \frac{1}{j\omega m + r + \frac{s}{j\omega}}. \tag{2.7}$$

This relation v/F in equation 2.7 is called mobility, which is denoted as $Y(\omega)$, and will be the type of FRF under examination in this thesis. It is also reciprocal to the mechanical impedance of the system, defined as $Z = F/v$ [13],[14].

2.3. Eigenfrequencies

When the imaginary part of the denominator in equation 2.7 becomes zero, mobility values reach infinity in numerical solutions. This condition in reality means a very high displacement, finite of course, which can happen for a certain frequency called Eigenfrequency or natural frequency, denoted by ω_0 . The physical meaning of that condition is a force compensation (same magnitude and direction) between the mass inertia and the spring stiffness at the natural frequency. As a result, a slight excitation force at ω_0 could lead to a high displacement or velocity [14].

The natural frequencies depend on the characteristics of every system under examination, i.e. the mass and spring stiffness. For the undamped case, considering that r=0, the Eigenfrequency for a simple mass-spring system is;

$$\omega_0 = \pm\sqrt{\frac{s}{m}}. \tag{2.8}$$

Resonance frequencies are the ones created by a forced excitation, like hitting and object with a hammer or applying a constant force signal with an exciter (e.g. shaker). The frequencies that have maxima in the FRF are the resonant ones.

2.4. Damping

The amplitude of resonance frequencies could be very high with low damping. Damping is the natural reduction of every oscillation due to energy losses, which means that

energy transformations happen, from vibrational to other energy forms like heat. These transformations generally happen due to viscoelastic, thermal and viscous friction effects.

Friction is an additional force proportional to velocity of the motion. For this reason, it is important to note that viscous damper coefficient r does not offer a convenient damping model for solids. In reality built up structures behave proportionally to displacement. Therefore a complex stiffness damping is used of the form $s(1 - j\eta)$ which represents a delay in the systems oscillation, causing an asynchronous motion effect [14],[15].

The term η stands for the loss factor, which is defined as a ratio between lost and reversible (potential) energy of the system;

$$\eta = \frac{E_{loss}}{2\pi E_{potential}}. \tag{2.9}$$

Then the mobility in this case be sipmlified as;

$$Y(\omega) = \frac{j\omega}{-\omega^2 m + s(1 - j\eta)}. \tag{2.10}$$

In Figure 2.2 the FRF of a SDoF and the effect of damping can be seen. The Mobility level is presented as a function of normalized frequency, i.e. the term ω/ω_0. The level value in decibel units is given as $L_Y = 20log(|Y/Y_0|)$ dB where Y_0=1 m/Ns as the reference value (normalization by 1). As illustrated, there is a stiffness controlled area below ω_0 with an upward trend and a mass dominated area above ω_0 with the opposite slope. The damping effect is mostly visible on the natural frequency, where it can be seen for different damping values. Overall, it leads to the amplitude reduction of any maximum [13],[14].

2.5. Modal Analysis

For every Eigenfrequency of a system there is a corresponding mode, which refers to a specific vibration pattern happening at the natural frequencies. Also called mode shapes or Eigenfunctions, modes depend on the geometry and material of the structure. They could be seen as energy storing oscillators which absorb part of the excitation energy to create their vibrational pattern. When there is an excitation close to a mode, that mode will absorb more energy and therefore will dominate the vibrational pattern.

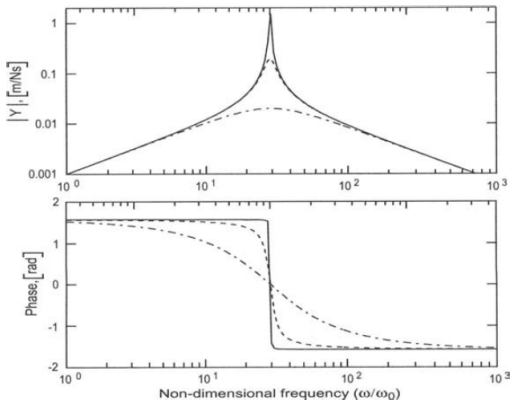

Figure 2.2.: Mobility and phase example of a SDoF system [13].

However, all modes can be excited every time but not with the same amplitude.

Examining the vibrational behavior of the system under excitation is a process called modal analysis and it can be very helpful to understand the dynamic properties, acquire modal shapes, eigenfrequencies and other important parameters of a structure such as the damping ratio. It is a way for engineers to calculate the FRF of a system by exciting the structure and measure the responses (transfer functions) in some other points.

There is a number of excitation ways like impact hammer, exciter, impulse ball, tyre dropping. A force transducer is used for the actual measurement of excitation force by the device at the excitation (driving) point. For the measurement points accelerometers are used and they also come in different sizes and sensitivities to capture vibrations depending on the structure's geometry and the wavelength of the frequencies under study.

Adding together every individual mode and its contribution (amplitude at every frequency) is a way to describe the behavior of a structure. Assuming orthogonality, it is valid to add separate modal energies and consider that they are not coupled. Therefore, the superposition of the mode functions can give the overall vibrational pattern [14].

For the case of a simply supported plate the Eigenfrequencies are;

$$\omega_n = \sqrt{\frac{B'}{m''}}\left[(\frac{n_1\pi}{l_1})^2 + (\frac{n_2\pi}{l_2})^2\right], \tag{2.11}$$

where $n = 1, 2, 3...$, denote the indices of the Eigenmodes. B' is the bending stiffness per

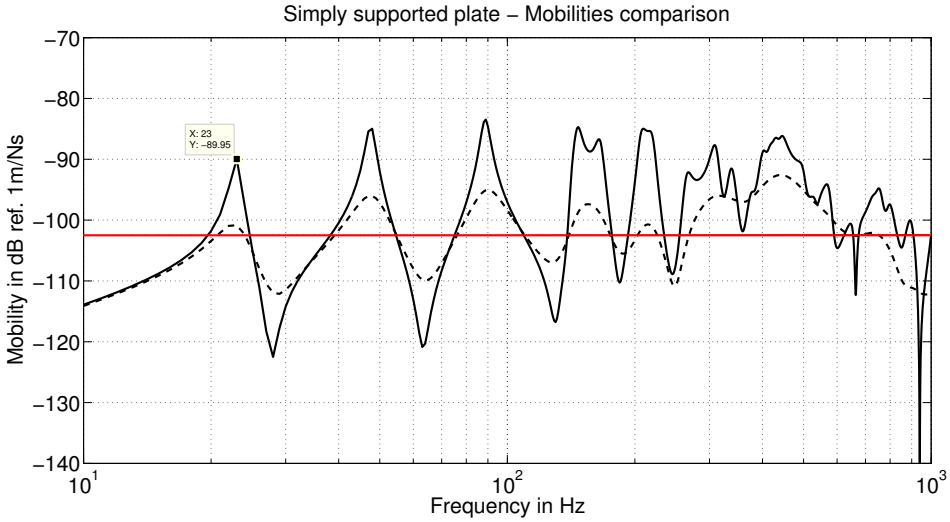

Figure 2.3.: Example of mobility plots for plate numerical models; red constant line for infinite, continuous and dashed lines for finite plates with loss factors 0.05 and 0.2 respectively. The case is for a timber plate with dimensions 4.5m*3.4m*0.1m. Excitation force is in the middle of the plate and the illustrated transfer point at the corner 0.2 m away from both sides.

unit length, m'' is the mass per unit area and l_1 and l_2 are the dimensions of the plate [13],[14].

The following expression describes the velocity on a plate under excitation by the force F_0. The driving point has the coordinates (x_0, y_0) and the transfer point (x, y).

$$v(x,y,\omega) \quad = \quad j\omega \frac{4}{\rho h l_1 l_2} \sum_n \frac{F_0(\omega) sin(\frac{n_1 \pi x_0}{l_1}) sin(\frac{n_2 \pi y_0}{l_2}) sin(\frac{n_1 \pi x}{l_1}) sin(\frac{n_2 \pi y}{l_2})}{(\omega_n^2(1+j\eta) - \omega^2)} \tag{2.12}$$

From expression 2.12 the driving or transfer point mobility can easily be calculated and also be compared with the mobility of an infinite plate which is given as;

$$Y_{inf}(\omega) \quad = \quad \frac{1}{8\sqrt{Bm''}}. \tag{2.13}$$

In Figure 2.3 the mobility levels for the above analyzed cases are presented. The effect of the loss factor is again prominent. For every natural frequency there is a modal pattern and the modes dominate with the resonance patterns the mobility curve. However, they fade out with increasing frequency, approaching the behavior of an infinite plate, due to the small size of the wavelength, which becomes comparable to the plate's thickness.

2.6. Waves in solids

There is a variety of waves propagating in solids which they differ from waves in the air due to the shear forces. Longitudinal (or compressional) waves are those propagating only to the horizontal direction, changing the volume but not the shape of the particle. Shear waves (or transversal) are the ones that change the shape but not the volume as presented in Figure 2.4. There are also torsional waves, which behave like transversal ones but in the tangential direction, quasi-longitudinal and bending waves. The last ones are regarded as most significant in this study and is analyzed further.

When studying structure-borne sound, bending waves are the most common to take place due to excitation and they dominate the low frequency range. Sound radiation from vibrating structures, such as a plate, is also mostly due to bending waves. This happens because there are many displacement elements vertical to the surface.

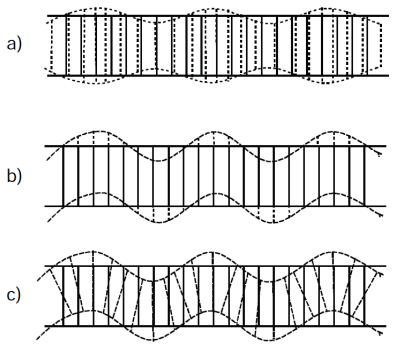

Figure 2.4.: Sketch of wave types in solids; a) quasi-longitudinal, b) shear wave and c) bending wave.

However, when bending waves become short, they usually transform into shear waves or longitudinal ones. The term short refers to the wavelength of high frequencies, which might be comparable to the dimensions of the structure under examination, like for example the thickness of a wall (plate). Transformations happen also when the geometry of a structure changes, like in a T-junction in building where there are perpendicular connections between columns, walls and floors. All these characteristics make the vibrational analyses in building acoustics very difficult in the crucial low frequency range [13],[14],[15].

2.7. Material Properties

The properties of every material are essential in physical and in numerical terms for modeling calculations. Some of them where mentioned before but not analyzed. In this section the necessary properties are explained briefly as they are being used further in this thesis, in the F.E.M. calculations.

The density, denoted as ρ, refers to the volumetric mass concentration of a material in a certain volume V. It is calculated as following in [kg/m^3];

$$\rho = \frac{m}{V}. \tag{2.14}$$

The elasticity or Young's modulus E, refers to a material's elastic deformation on an axis while forces are acting on it. Consequently, the stiffer the material the bigger the modulus value. Numerically E is expressed as stress σ to strain ε ratio in the direction of applied force in [Pa];

$$E = \frac{\sigma_x}{\varepsilon_x}. \tag{2.15}$$

The Poisson effect refers to the reaction of a material at the different sides of the compression axis, like the stretching effects on a rubber. The Poisson's number, v, is the ratio of longitudinal to lateral deformations with respect to a certain axis, numerically expressed as;

$$\nu = -\frac{\partial \varepsilon_z}{\partial \varepsilon_x}. \tag{2.16}$$

Bending stiffness B can be calculated then as the following expression;

$$B = \frac{E}{1-\nu^2} I, \tag{2.17}$$

where I in the cross-sectional area moment of Inertia;

$$I = \frac{h^3}{12} \tag{2.18}$$

with h denoting the plate's thickness.

Finally, the loss factor η, as analyzed previously, is responsible for the damping effects of the system. So it is a kind of energy absorption coefficient and its values are always less than one as they refer to the percentage of lost energy [11],[13],[14].

2.8. The Finite Element Method

Previously the numerical solution of a transfer mobility on a plate under force excitation was presented (Figure 2.3). However, the structures under study are many times too complicated to approximate their response using simple beam or plate numerical models. Finite Element modeling is used then, as the standard engineering tool to acquire complex numerical solutions using partial differential equations in several domains.

According to Finite Element Method (F.E.M.) a structure is split into parts, the finite elements. The physical behavior of a system can be approximated by the calculations for every individual element, according to the right numerical solutions. All separate results can be combined afterwards with the proper conditions (equilibrium, continuum) and the coupled subsystems can provide the overall solution.

In few words the essential steps of F.E.M. are;
- CAD modeling; Building the structure's geometry.
- Meshing; Subdividing the geometry in finite elements and setting up the nodes for the calculations.
- Applying boundary conditions to the model (e.g. clamped sides of a plate) and the right differential equations (software module).
- Defining all inputs of the system (e.g. point force).
- Selection of a software solver (e.g. stationary solver).
- Defining the expected outcome (e.g. stress, displacement).

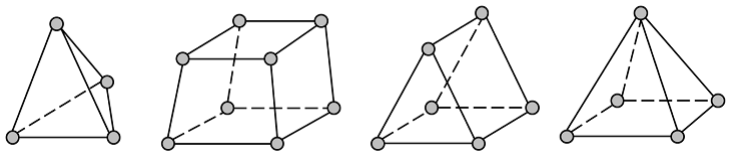

Figure 2.5.: The four meshing elements of Comsol; tetrahedra (tets), hexahedra (bricks), triangular prismatics (prisms), pyramid elements [10].

The process of discretizing the geometry of a structure is called meshing. In Figure 2.5 the basic types of meshing elements in COMSOL are illustrated. The grey points are the nodes of the elements. The meshing elements can be used in combinations of types and density, according to the demands of every study. A higher density of a mesh corresponds to more detailed calculations and hence better results acquired from the F.E. model. Therefore, finer meshing can be applied where more information is needed.

An example of a F.E. problem is presented in Figure 2.6. The boundary condition for this case is a clamped condition on the one side of the plate. The input is an excitation on the other side of the plate with distributed load (left sketch) or concentrated point load (right sketch). Two cases of meshing in COMSOL (normal and finer) are illustrated as well.

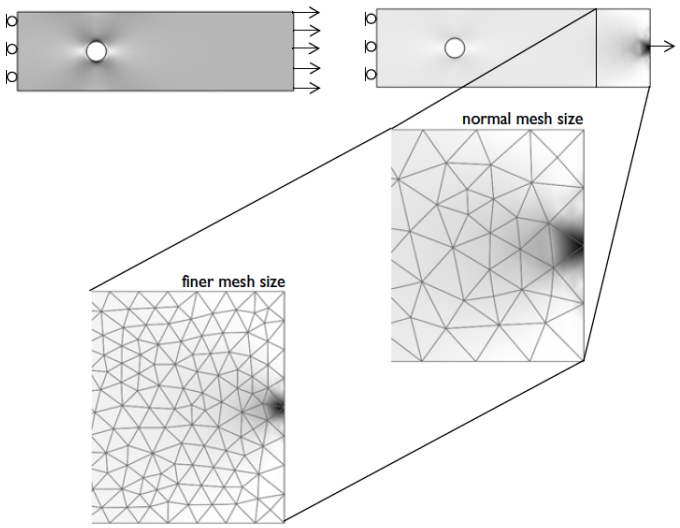

Figure 2.6.: Example case of a plate with a hole in COMSOL. Distributed and point load for the right and the left case respectively [16].

Detailed information about the mathematical formulations in F.E.M. can be found widely in the literature and specifically for COMSOL's structural module used in this study in [16]. However there are many theory variations due to different applications. Another relevant example of F.E. modeling of a simple clamped plate excited by force is presented in [17] and compared to measured results for further validation.

A complete F.E.M. model was built for the vibrational study in this thesis, using COMSOL Multiphysics software. The module for structural dynamics calculations was used for a linear static analysis. Static means that there is no variation of the parameters over time. The input force at the driving point as well as some boundary conditions were defined and the displacements at the transfer points were collected. A thorough description of the F.E. model developed in this thesis is given in a following chapter.

2.9. Sound Radiation

Besides structure-borne sound in solids, there are also interactions of the structure and the surrounding environment. In simple words, every vibrating surface radiates sound. Given a bending wave excitation, there will be a velocity distribution over the surface, like in the case analyzed in this study. And that surface is the connecting interface between two propagating media for the oscillations, the solid and the gas.

The radiation factor, σ, is used to characterize the efficiency of a surface as a sound radiator. It is defined as:

$$\sigma = \frac{W_{rad}}{\rho_0 c_0 S \langle \widehat{u}^2 \rangle} \tag{2.19}$$

where *Wrad* is the power radiated from the surface, S is the surface area and $\langle \widehat{u}^2 \rangle$ is the mean square velocity amplitude of the radiating plate, averaged in the spatial domain. The term $\rho_0 c_0$ refers to the density and speed of sound for the surrounding medium, i.e. the air usually. It is called the characteristic impedance, also denoted as Z_0 [13],[14],[15].

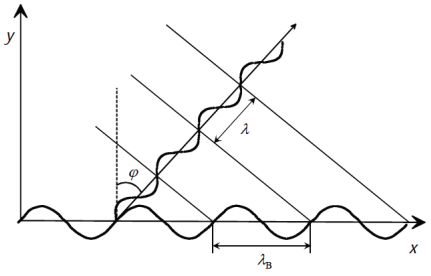

Figure 2.7.: Sketch of radiation efficiency for plates.

Sound radiation happens at a certain angle ϕ when the bending wavelength in solids λ_b is bigger than the one in the gas, as illustrated in Figure 2.7. The condition where λ_b = λ_{air} happens at the critical frequency f_c, which is calculated as;

$$f_c = \frac{c_0^2}{2\pi} \sqrt{\frac{m''}{B'}} \tag{2.20}$$

and sound radiation takes place above that. According to the theory, for infinite plates there is no sound radiation below f_c (σ = 0) but it is infinite at f_c and reaches 1

above f_c. However in real cases for finite plates things change a bit, i.e. the radiation efficiency at f_c is maximum, higher than unity but finite of course. Below f_c there is still sound radiation of very low levels which happens due to the bending nearfields.

Bending waves have a frequency dependent speed of sound, which makes their wavelength smaller below f_c, hence there is no appropriate angle for the projection of the bending wavelength to the gas. In that region where $\lambda_b < \lambda_{air}$ short-circuits appear where the air moves locally from positive displacement areas to the negative ones and vice versa. So these movements of air cancel each other dissipating sound pressure fields while creating dipole or quadrapole patterns. For a finite plate case, this condition is not fulfilled close to the edges of the surface, so there will be some sound radiation from the side areas where cancelation is impossible, hence nearfields exist.

Finally, above f_c, where $\lambda_b > \lambda_{air}$ there is sound radiation at a certain angle for both finite and infinite plate cases. In general, sound radiation depends on the critical frequency, the plate's dimensions, the boundary conditions and the excitation, i.e. which modes of the structure are excited.

For the case of a plate under excitation the calculation of radiation efficiency is not straightforward. The use of an averaged radiation factor (in 1/3 octave bands) is essential because there will be contributions from different modes with several amplitudes in every band. Therefore some numerical approximations are used in these cases, as stated in the literature [15],[18]. In this study, the following expressions established by Leppington et. al. (1982) for σ were used. For $f < f_c$, which is also the range in this study case, the radiation factor is calculated as;

$$\sigma = \frac{Uc_0}{2\pi^2\sqrt{ff_c}S\sqrt{\chi^2-1}}\left(\ln\frac{\chi+1}{\chi-1}+\frac{2\chi}{\chi^2-1}\right). \tag{2.21}$$

For $f \approx \mathrm{f}_c$ σ is given as;

$$\sigma = \sqrt{\frac{2\pi f}{c}}\sqrt{a}(0.5-0.15\frac{a}{b}), \tag{2.22}$$

and finally for $f > f_c$;

$$\sigma = \frac{1}{\sqrt{1-\frac{f_c}{f}}}. \tag{2.23}$$

3. Implementation

3.1. Measurement of the Test Floor

The measurements in the test room, which is the only complete apartment of the building under investigation at the time of this thesis, took place at Fristad. For the investigation of the building's floor junction, a template including measurement positioning from the research program Acuwood [4] was used, which is presented in Figure 3.1, together with all points used.

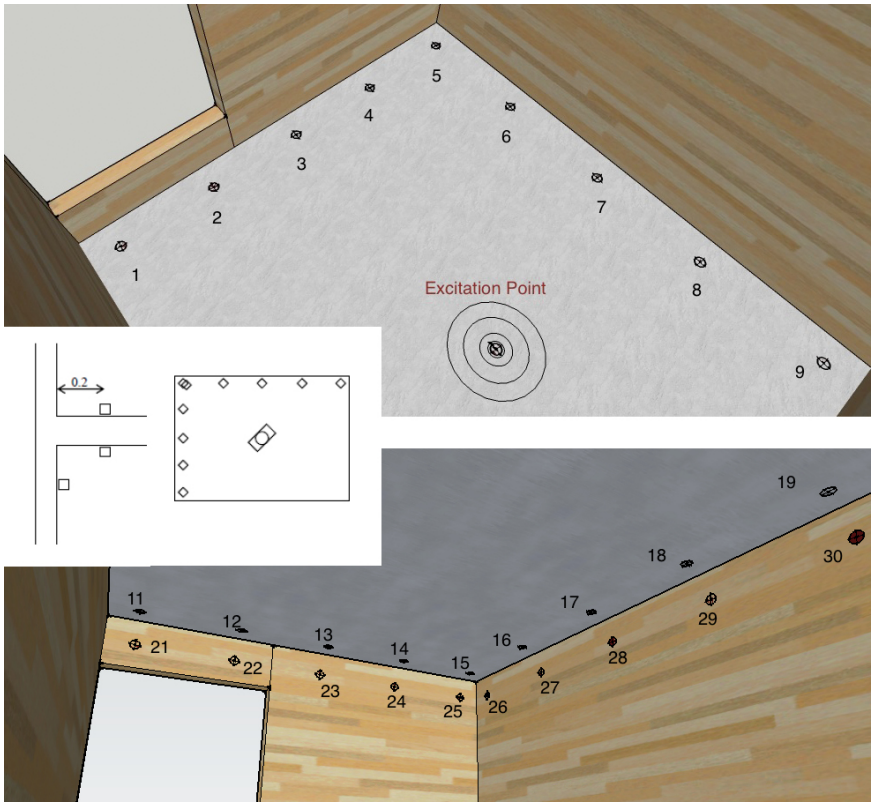

Figure 3.1.: Measurement points on the test floor and the ceiling and walls below that (0.2m distance from the edges).

The performed measurement session includes transfer point mobilities on the floor under excitation, on the ceiling and the walls of the vertically adjacent apartment below. So flanking transmission is also of interest, i.e. the indirect transmission from the specimen (the multilayered slab) to the walls.

All accelerometers were connected to the data acquisition station NI cDAQ 9188 (includes 8 subinterfaces connected type cDAQ 9234), without any external amplification and calibrated with the B&K calibration exciter for every axis before measuring. The impact hammer was also connected to the NI interface directly. The software used for the acquisition was ModalView [19] and the sampling frequency was 2.56 kHz with a frequency step of 0.25 Hz. The final FRF acquisition is the averaged result of 30 excitations.

The measurement was performed in sets of 5 transfer points corresponding to the point arrays 1-5, 5-9, 11-15, 15-19, 21-25 and 26-30. For every excitation iteration there was a driving point measurement as well. The measurement setup for the point array 5-9 is captured in Figure 3.2 and the list of equipments is presented in Table 3.1. Detailed photos of every submeasurement can be found in the Appendix.

Table 3.1.: List of equipment

Equipment name	Model specification	Serial no.
Laptop	Hewlett Packard	———
Data acquisition board	NI DAQ 9188	1820FF7
Impact hammer	Dytran Instruments LIXIE	5803A
Calibration Exciter	B&K Type 4292	1145133
Triaxial accelerometer	PCB Piezotronics 356A16	LW147922
Triaxial accelerometer	PCB Piezotronics 356A16	LW147923
Triaxial accelerometer	PCB Piezotronics 356A16	LW147924
Triaxial accelerometer	PCB Piezotronics 356A16	LW147954
Triaxial accelerometer	PCB Piezotronics 356A16	LW147955

Figure 3.2.: Photo of the measurement at points 5-9 on the floor.

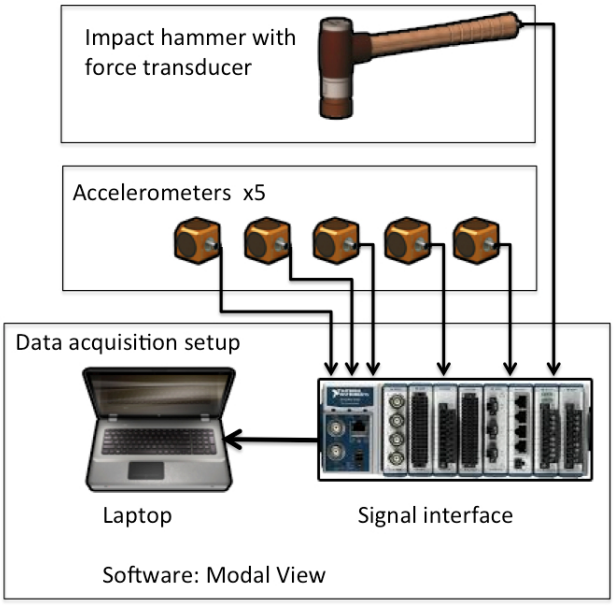

Figure 3.3.: Sketch illustrating the measurement setup

3.2. The F.E.M. Model Setup

For the setup of the F.E. model some approximations need to be done according to each study case and the corresponding physics theory. Numerical models deviate from reality to some extends due to the method's precision but most importantly because of the approximations and assumptions. Therefore, the latter need to be wisely performed in the design of the model. In cases related to structural dynamics for vibration prediction, such as in this thesis, certain parts like the structures geometry, the material properties, the boundary conditions and the meshing (number of elements, degrees of freedom) are of great interest.

The first step was the design of the F.E. model of the test structure, which was based on the construction plans acquired by Fristadsbygg, as shown previously. There was not any important change, especially concerning the plate layers of the floor. Different dimensions would affect the calculation of the structural modes, which depend on the geometry. The model was built in AutoCAD in '.dwg' format, InventorFusion was used to transform the file to '.stp' format and then it was imported in COMSOL Multiphysics. The CAD file of the model is illustrated in Figure 3.4.

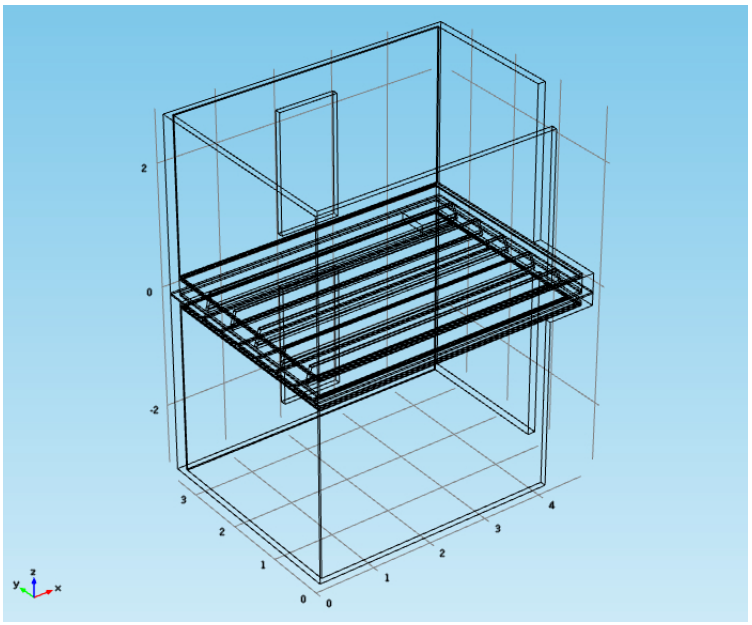

Figure 3.4.: Image of the CAD wireframe geometry designed for the F.E. model

Regarding the approximations, some parts of the actual structure, as shown in the design plans, were ignored or integrated in the dominant parts of the model. All lay-

ers and materials were included, except some mineral wool parts, the windows and some additional gypsum wall layers. Those decisions are based on the materials properties, their position on the structure and the role they could play within the F.E. model.

Mineral wool is the softest material compared to the other ones and it is not rigidly connected to the other stiff parts but rather assembled. It is used for sound insulation, not vibration isolation so it was excluded from the model. It has a maximum thickness of 222 mm which barely affects the frequencies of 10 - 200 Hz under study. Therefore, its contribution to the dynamic simulation would not have a big influence. However, the smaller wool layer above the aluminum profile was modeled to fulfil the condition for some connection of the layers between the CLT floor plate and the gypsum ceiling below. It was also required for approximating the air cavity in the effect of the double wall resonance.

The windows were also excluded from the walls and replaced by CLT because their connection to the floor under study is not direct. They also have details like wooden frames and double glass layers which could not integrate easily or accurately in the model. The door openings in the walls which can be seen in the plans (Figure 3.4) are used only by the workers during the construction. They are filled, after finishing the construction, with mineral wool and they stay hidden behind the gypsum wall. That construction characteristic was kept and modeled as a void in the CLT element.

Figure 3.5.: Photo of the gypsum walls in the floor, which include structural parts as pipes or ventilation that could not be integrated in the F.E. model.

Most of the gypsum walls of the real construction were not included in the model ge-

ometry as well. They are thin layers compared to CLT elements (26 mm) and although they affect the floor being rigidly connected, the model would become too detailed. There are also implications concerning the parts inside gypsum walls for the test room, which could not be integrated in the model. Some of them enclose the water pipe and cable connections, as presented in Figure 3.5. Only the gypsum walls next to the transfer points 5-9 and 15-19 were included in the F.E. model. The other wall side next to the points 1-5 and 11-15 consists of bare CLT due to the architectural design. Consequently, if the above analyzed simplifications did not happen, the model and simulations would be more complicated and time-demanding.

The material parameters used in the model are presented in Table 2 and they were collected from certain parts of literature, such as [13],[15],[20]. However, they had to be changed in later simulations so they could match the corresponding modes acquired by the field measurements, as shown in Table 3. This process of tuning is justified because the F.E.M. usually offers overestimated results. Another assumption that took part concerns the linearity and isotropic behavior of the materials, so constant values were used for all their properties.

Table 3.2.: Material properties from literature

Material	E (Pa)	$\rho(kg/m^3)$	ν	η
CLT	7e9	480	0.44	0.1
Chipboard	3.5e9	600	0.2	0.01
Ballast	30e6	1600	0.35	0.2
Sylomer	3.5e5	300	0.3	0.1
Min.Wool	2.2e5	140	0.1	0.1
Aluminium	60e9	2700	0.3	0.05
Gypsum	7e9	1200	0.3	0.01
Screed	2e9	1200	0.2	0.05

The next step is the meshing which refers to the discretization of the geometry in finite elements before the calculations. As a rule of thumb, 6-10 elements per wavelength are demanded for a valid simulation. For the frequency range used this is not a difficult requirement. However, attention had to be given at the meshing of layers with small dimensions, for example the Elastomer parts with the minimum height of 12 mm.

The construction of a balanced mesh includes a sufficient resolution without too many elements to avoid complications. The industrial settings of COMSOL included mesh generation options (like normal, coarse, fine or finer) and element type selection

Table 3.3.: Material properties tuned in the F.E. model

Material	E (Pa)	$\rho(kg/m^3)$	ν	η
CLT	4e9	400	0.4	0.2
Chipboard	2e9	300	0.2	0.05
Ballast	10e6	1000	0.3	0.2
Sylomer	2e5	300	0.3	0.1
Min.Wool	1e5	140	0.1	0.1
Aluminium	40e9	2700	0.3	0.05
Gypsum	4e9	800	0.3	0.03
Screed	1e9	1000	0.2	0.1

(like tetrahedral, triangular or hexahedral). They give also the possibility for the user to select minimum or maximum dimensions of the elements. For this study model, a normal mesh was used with the standard tetrahedral elements for dynamic investigation, as illustrated in Figure 3.6. Then a manual meshing was developed for the surface layers of the floor, which include more details and they are more important for the acquisition of the transfer point results. In the slab, the mesh grid became as dense as needed to match the dimensions of thin layers. That seemed to be the best optimization between resolution and the overall number of elements.

For the whole setup of the physics and the boundary conditions in the software, the structural dynamics module was used. An input force at the driving point, on the center of the floor plate, was applied with a value of 100 N. Constraints of zero displacement were set up for the thin surface boundaries above and below the walls, which in reality are connected to other CLT construction parts directly or with elastomer in between.

Different models were developed and numerous simulations took place during the study. But for the purposes of this study, all the information of this chapter refer to the most optimized model. The final model has exactly 615990 degrees of freedom and the calculation time needed was about 17 hours. The stationary solver was used for the linear static response F.E. analysis.

The outcome of the calculations was the set of displacements at the transfer points, which were chosen in the same geometrical positions with the measurement transfer points. All the data were exported from COMSOL Multiphysics as '.txt' files. Then they were imported in MATLAB [21], the mobility levels in dB (referenced to 1 m/Ns) were calculated according to the theory (expression 2.7) and post-processed for presentation.

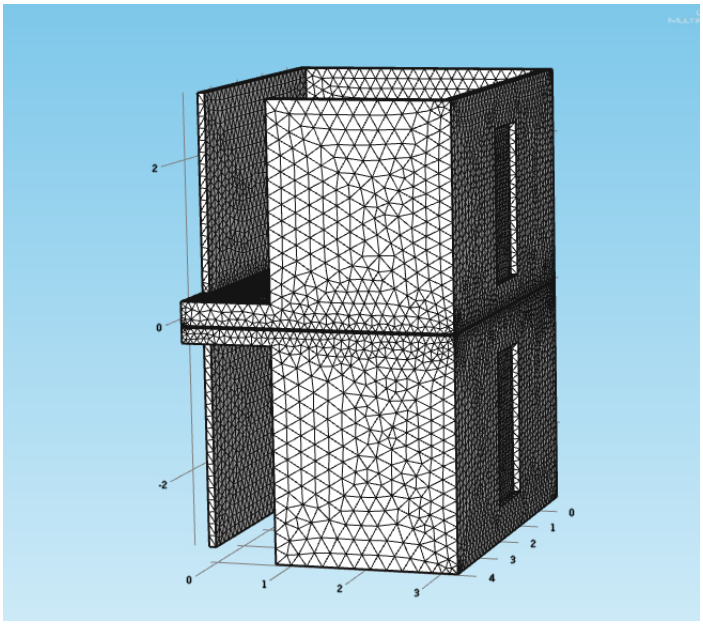

Figure 3.6.: Image presenting the Finite Element model in COMSOL Multiphysics, after the process of meshing. The elements get smaller at the multilayered floor area for better resolution and accuracy in the results.

3.3. Impact sound levels approximation

The last step of the calculations was a numerical approximation of the impact sound levels at the room below the test structure under excitation. The aim was to compare the calculated results with the ones measured by WSP as presented later in the "Results and Data" chapter.

The radiation efficiency was determined for our range where $f < f_c$ with equation 2.21. However, that expression is an approximation. As for the test structure, the ceiling's modes are also disrupted by the metal supporting grid (spacing $\sim$ 60 cm), which is rigidly connected to the walls. Hence, the radiation behavior of that surface with that structural conditions is not easily predictable or approachable.

The radiated power from the ceiling to the room below the test floor had to be calculated and linked to expression 2.19. The averaged velocity at the ceiling's surface (Points 11-19) was acquired from the F.E.M. results. For valid averaging more points are demanded and therefore 56 additional transfer points were used to calculate the mean squared velocity of the plate $\langle \hat{u}^2 \rangle$. All the ceiling's surface points used for the sound radiation setup are illustrated in Figure 3.8.

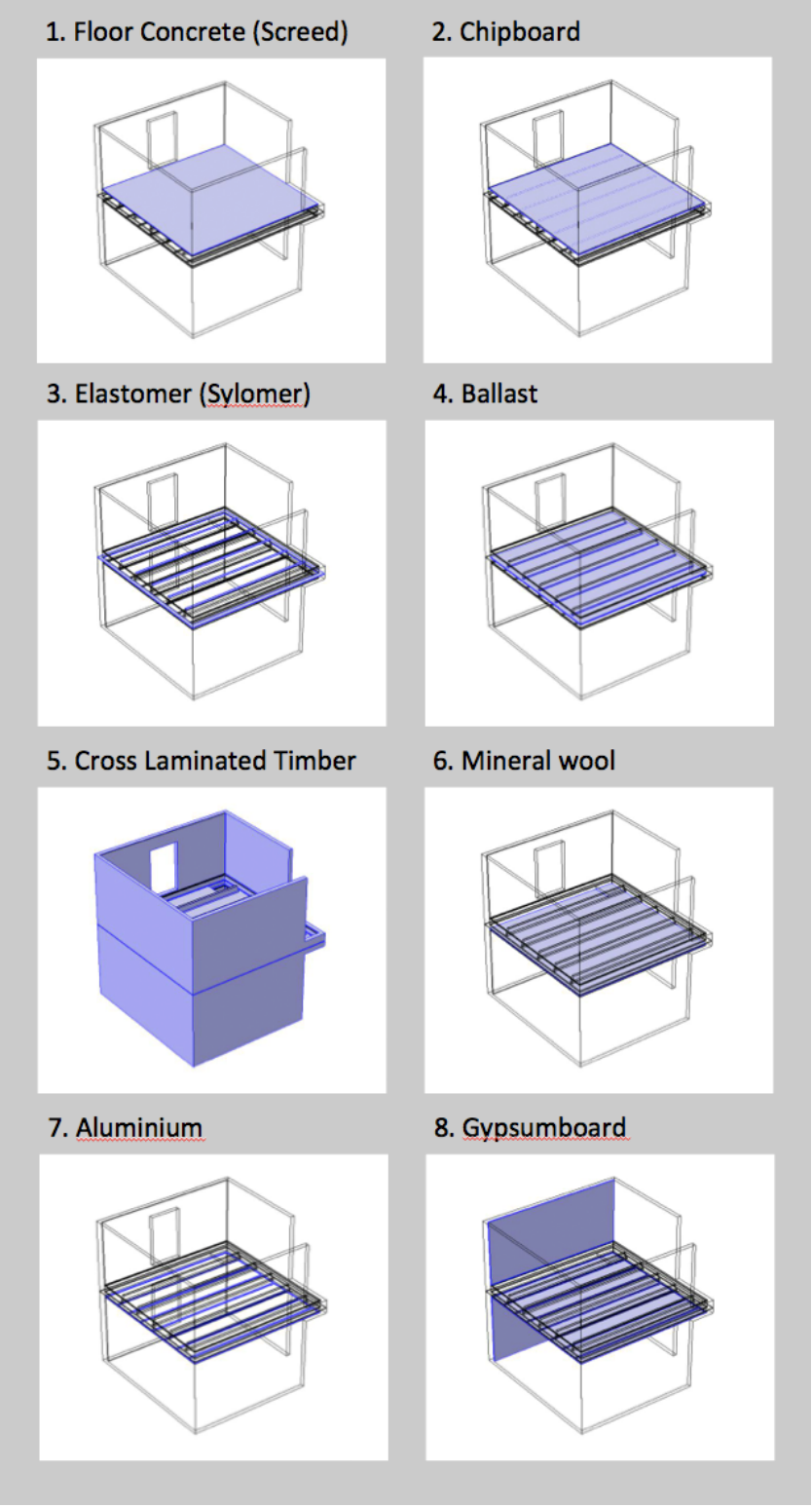

Figure 3.7.: Image presenting the different material layers and their position in the Finite Element model.

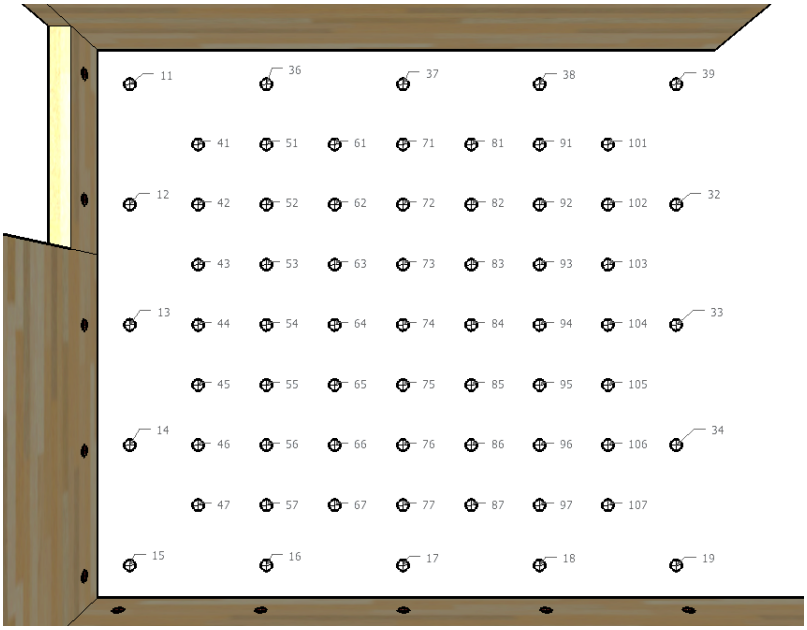

Figure 3.8.: Transfer points used for acquiring velocities to calculate the radiated sound from the ceiling.

Another numerical approximation concerning the standardized tapping machine was involved in the calculations. The machine has 5 hammers with mass m_h = 0.5 kg each, falling from a height H = 0.04 m with a frequency f_t = 10 Hz. The tapping machine force $F_{t\Delta f}$ in 1/3 octave bands was used to scale $\langle \widehat{u}^2 \rangle$ so as to match the one from the real impact sound measurements. According to Vigran this force can be calculated as;

$$\widehat{F_{t\Delta f}}^2 = 2 f_t I_t^2 \Delta f, \tag{3.1}$$

where I_t is the machine's impulse given as;

$$I = m_h \sqrt{2gH}. \tag{3.2}$$

The term g above refres to the gravitational acceleration which has a value of 9.8 m/s^2[15].

After the above calculations the averaged radiated power in 1/3 octaves can be acquired from equation 2.19. Then the sound power levels L_w are given as;

$$L_w = 10 \log(\frac{W}{10^{-12}}). \tag{3.3}$$

The sound pressure levels L_p (referenced to 2e-5 Pa) can then be approached as

$$L_p = L_w + 10\log(\frac{4}{A}), \tag{3.4}$$

where A is the absorption area derived by Sabine's expression as;

$$A = \frac{0.16V_{room}}{T_{60}}. \tag{3.5}$$

The terms T_{60} and V_{room} denote the reverberation time (impulse response drop by 60 dB) and the volume of the room respectively.

Finally, the normalized impact sound levels were calculated as

$$Ln = Lp + 10\log(\frac{A}{A_0}), \tag{3.6}$$

where A_0 = 10 is the reference value for the absorption area [11],[22].

4. Results and Data

In this section, the complete results of the thesis are presented all together and they are discussed in the next chapter.

In the first subsection, the initial measurements outcome is illustrated in mobility and coherence graphs, concerning the building's junction under study. The aim of these graphs is to give an overall impression for the data acquired and the structure's vibrational behavior. Therefore, the whole frequency spectrum of the measurement, 10-2000 Hz, is visible. The differences among driving point (measured next to the excitation point) and transfer point mobilities can be seen in a presented sequence and be compared. The validity of the mobilities is shown as well in the coherence plots.

The second subsection, includes the significant comparisons between the measurements and the results acquired by the F.E.M. simulations in Comsol. The frequency range presented is the one under investigation, no higher than 200 Hz. There the behavior of the F.E.M. model can be evaluated according to how well approximates the real structure's dynamic response and hence to what extend it could be regarded as valid. Every transfer point measurement is plotted in individual graphs with the corresponding results from the F.E. model for straightforward comparison and understanding.

The final subsection presents the comparison between calculated and measured impact sound levels, in the same study range 10-200 Hz. The impact sound insulation measurements were performed by WSP according to ISO 140-7 and evaluated according to ISO 717-2 [23],[24]. The calculated results are based on the averaged velocities acquired by the F.E. model, as analyzed above in Chapter 3.3 and the sound radiation approximations.

4.1. Measurements of the test construction
Mobility graphs in narrow band 10-2000 Hz

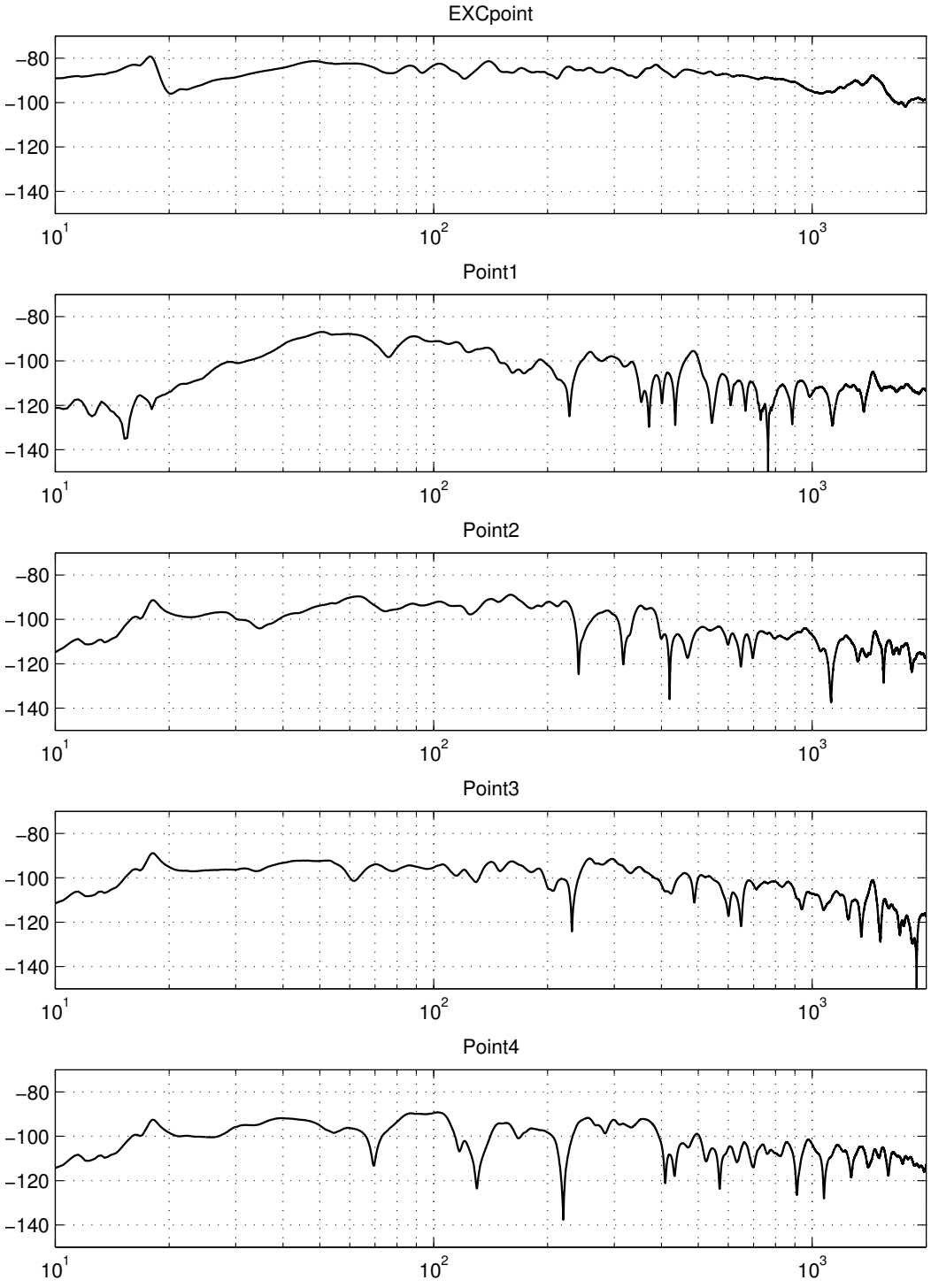

Figure 4.1.: Measurements of the construction; driving point (EXC) and transfer points 1 to 4. Mobility [dB ref. 1m/Ns] in vertical axis plotted over frequency [Hz, range; 10-2000] in horizontal axis.

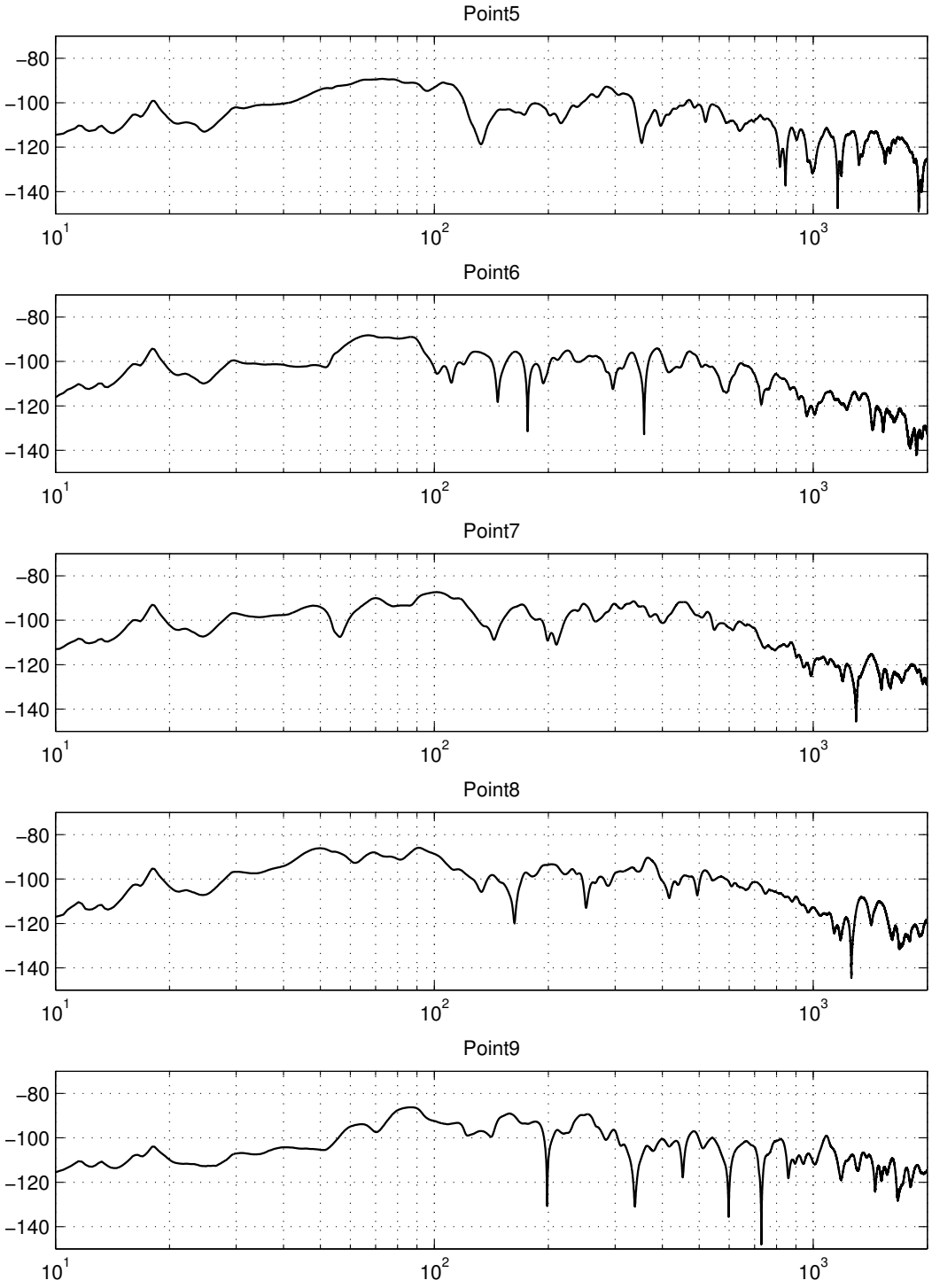

Figure 4.2.: Measurements of the construction; transfer points 5 to 9. Mobility [dB ref. 1m/Ns] in vertical axis plotted over frequency [Hz, range; 10-2000] in horizontal axis.

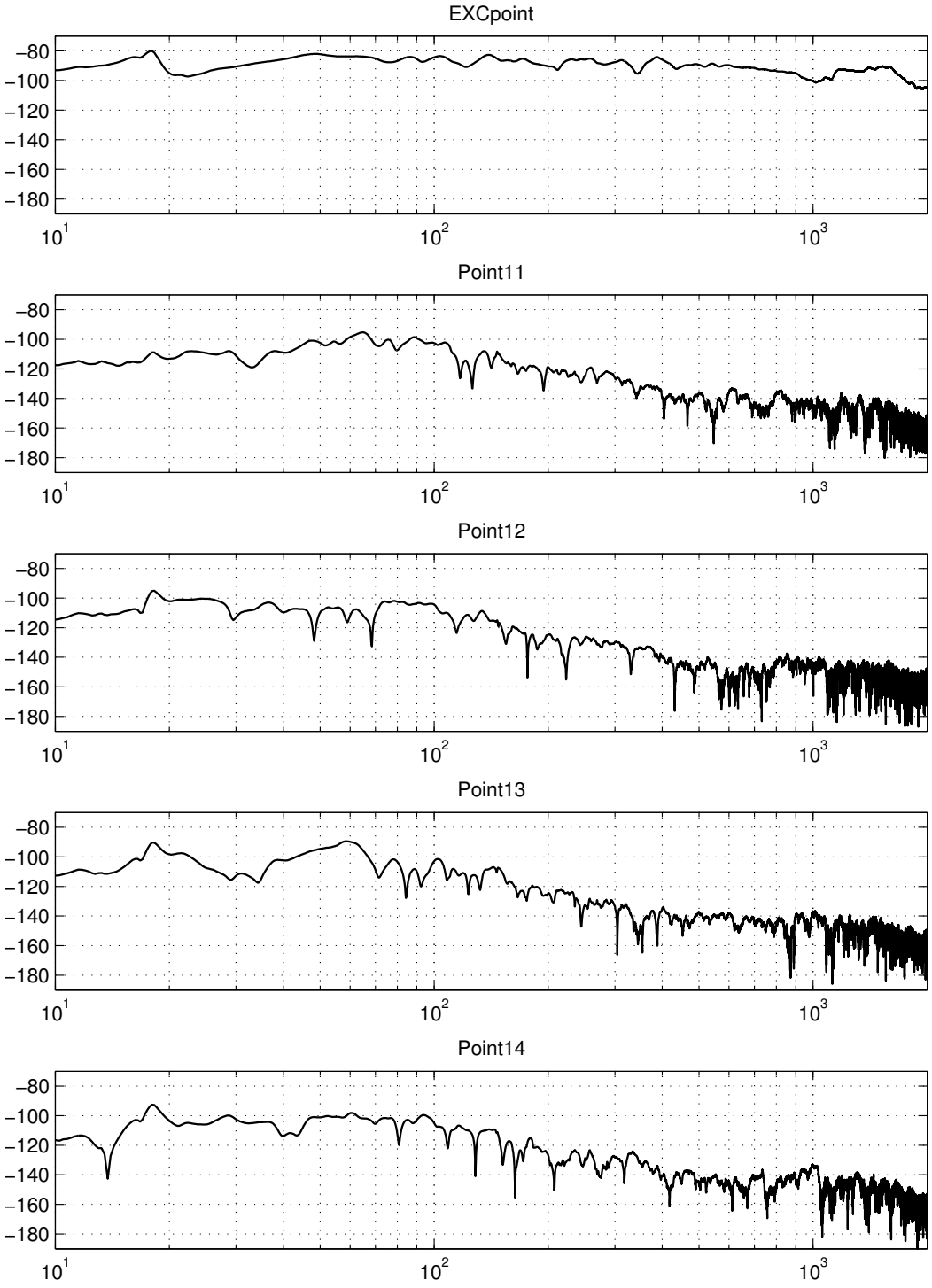

Figure 4.3.: Measurements of the construction; driving point (EXC) and transfer points 11 to 14. Mobility [dB ref. 1m/Ns] in vertical axis plotted over frequency [Hz, range; 10-2000] in horizontal axis.

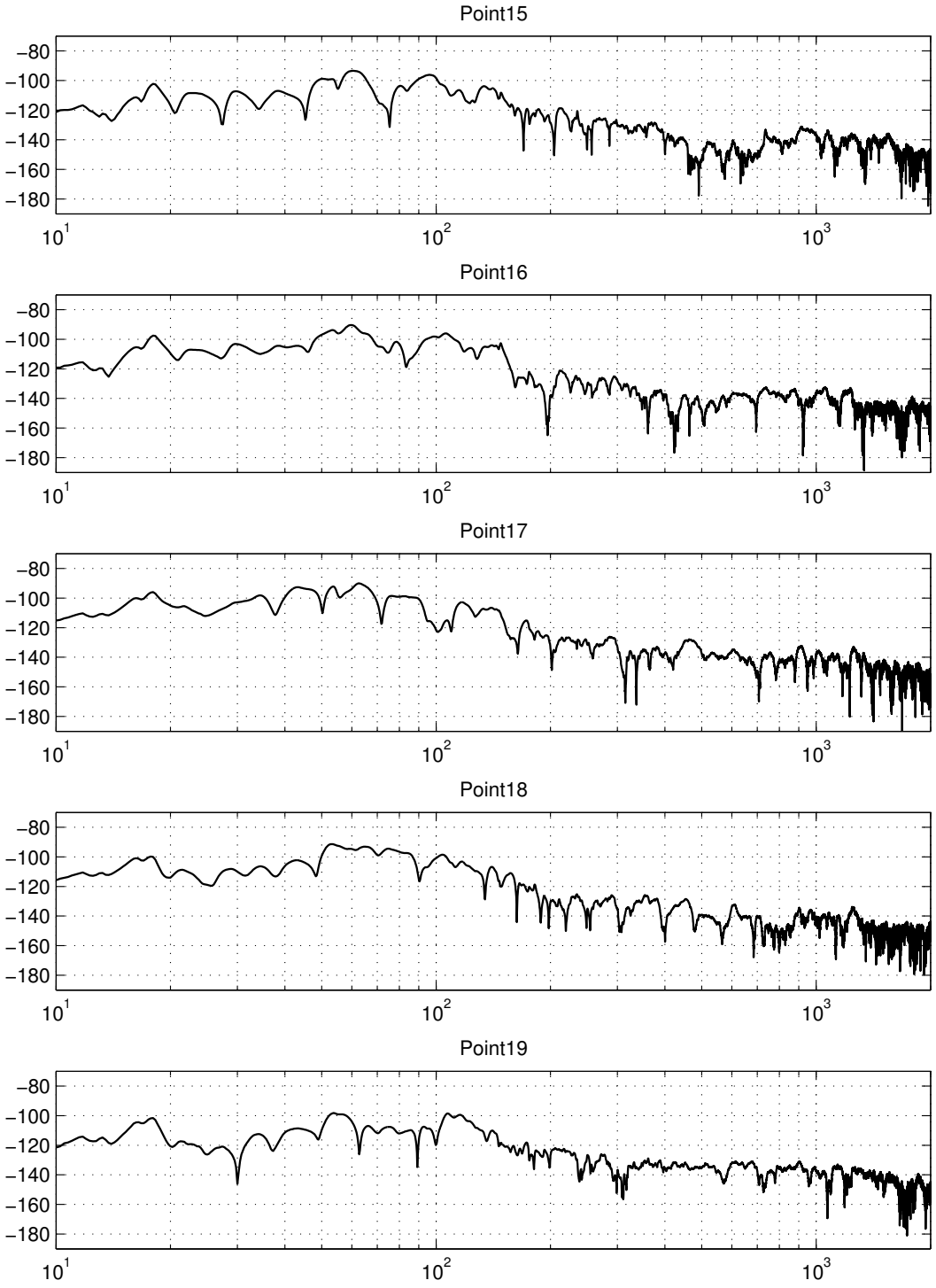

Figure 4.4.: Measurements of the construction; transfer points 15 to 19. Mobility [dB ref. 1m/Ns] in vertical axis plotted over frequency [Hz, range; 10-2000] in horizontal axis.

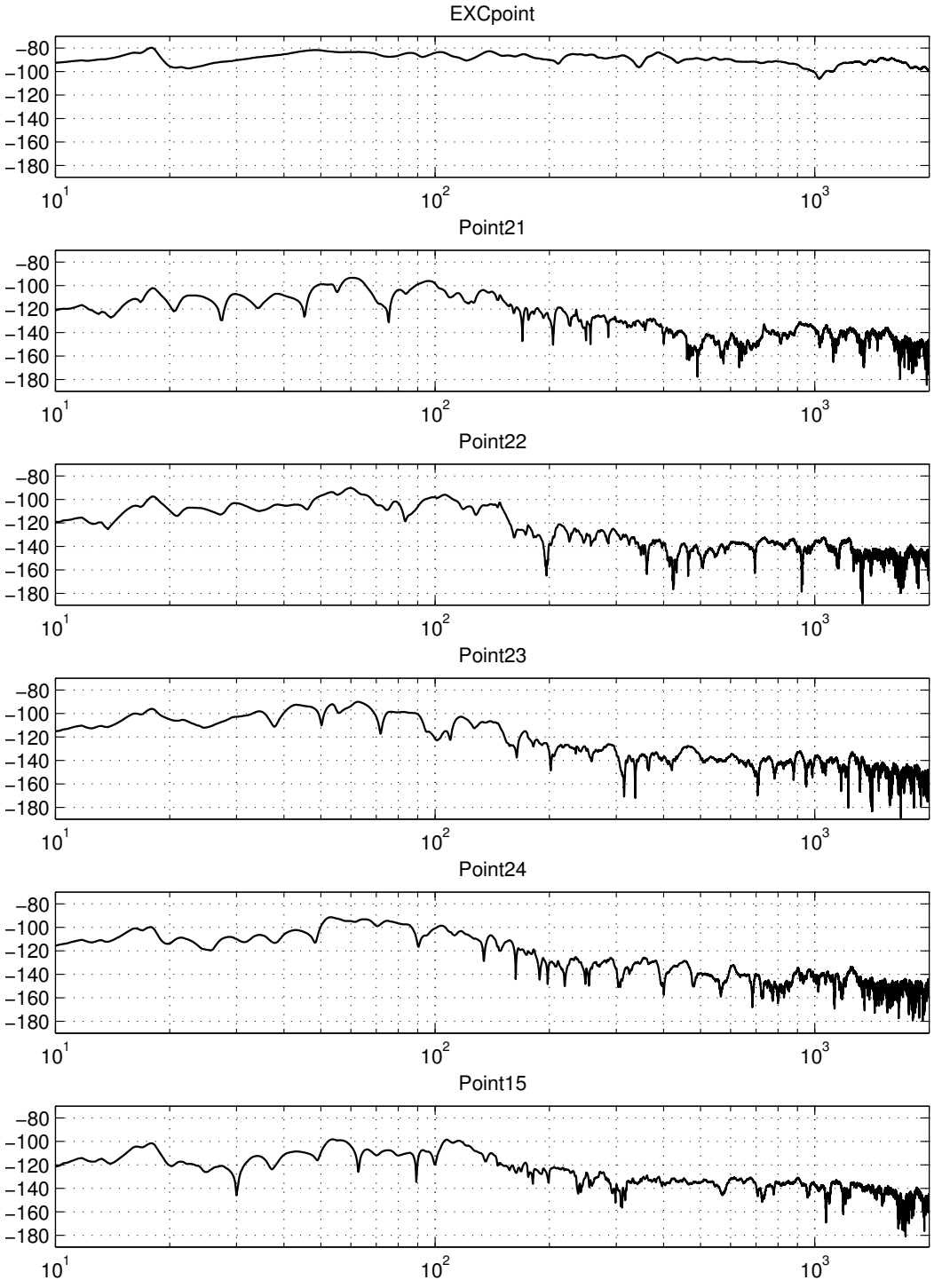

Figure 4.5.: Measurements of the construction; driving point (EXC) and transfer points 21 to 25. Mobility [dB ref. 1m/Ns] in vertical axis plotted over frequency [Hz, range; 10-2000] in horizontal axis.

4.2. Comparison graphs; Measured and simulated mobility levels and impact noise levels by F.E.M.

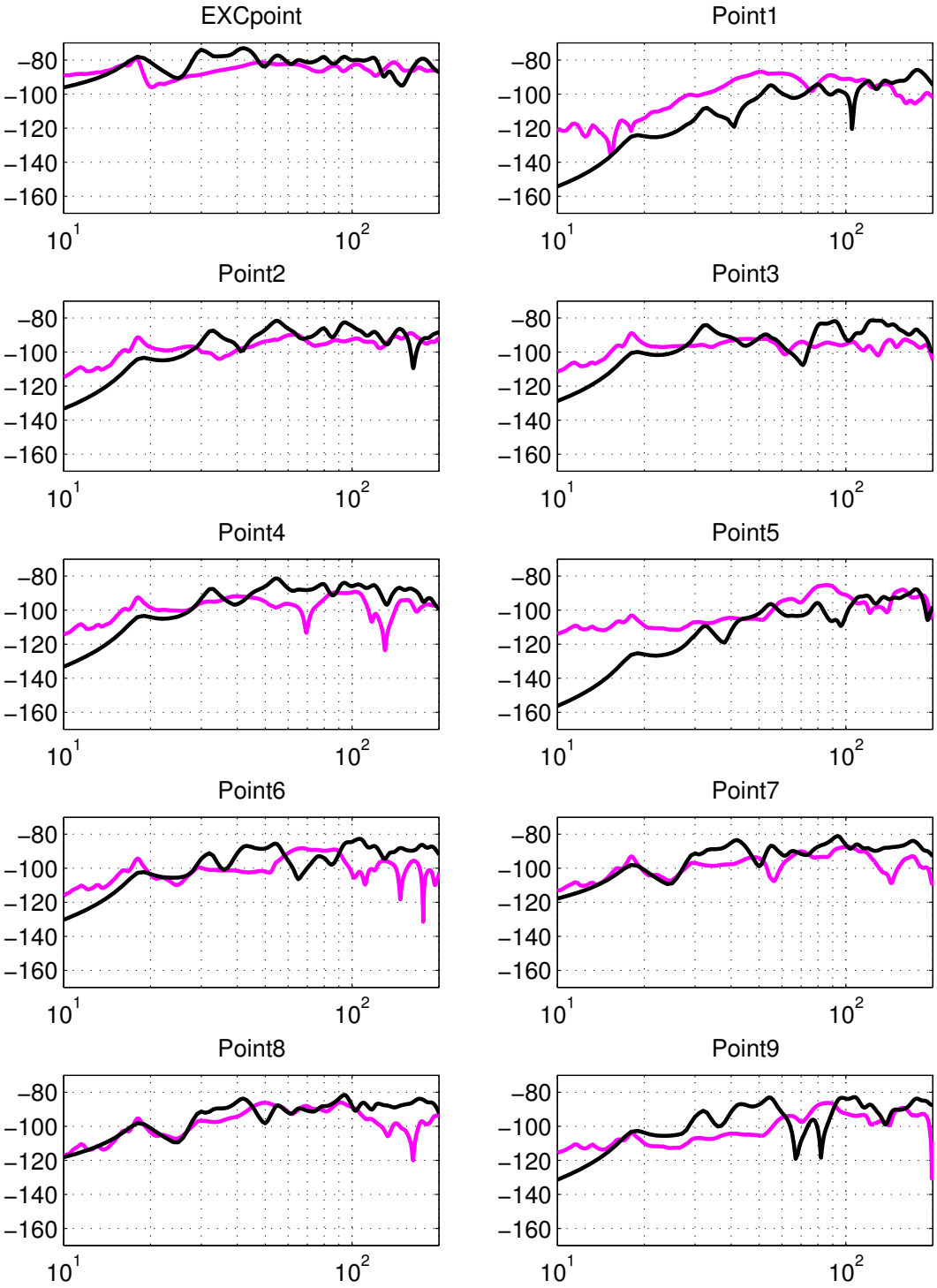

Figure 4.6.: Data comparison for points 1 to 9; thin purple lines for measured results and thick black for modeled by F.E.M. Mobility [dB ref. 1m/Ns] in vertical axis plotted over frequency [Hz, range; 10-200] in horizontal axis.

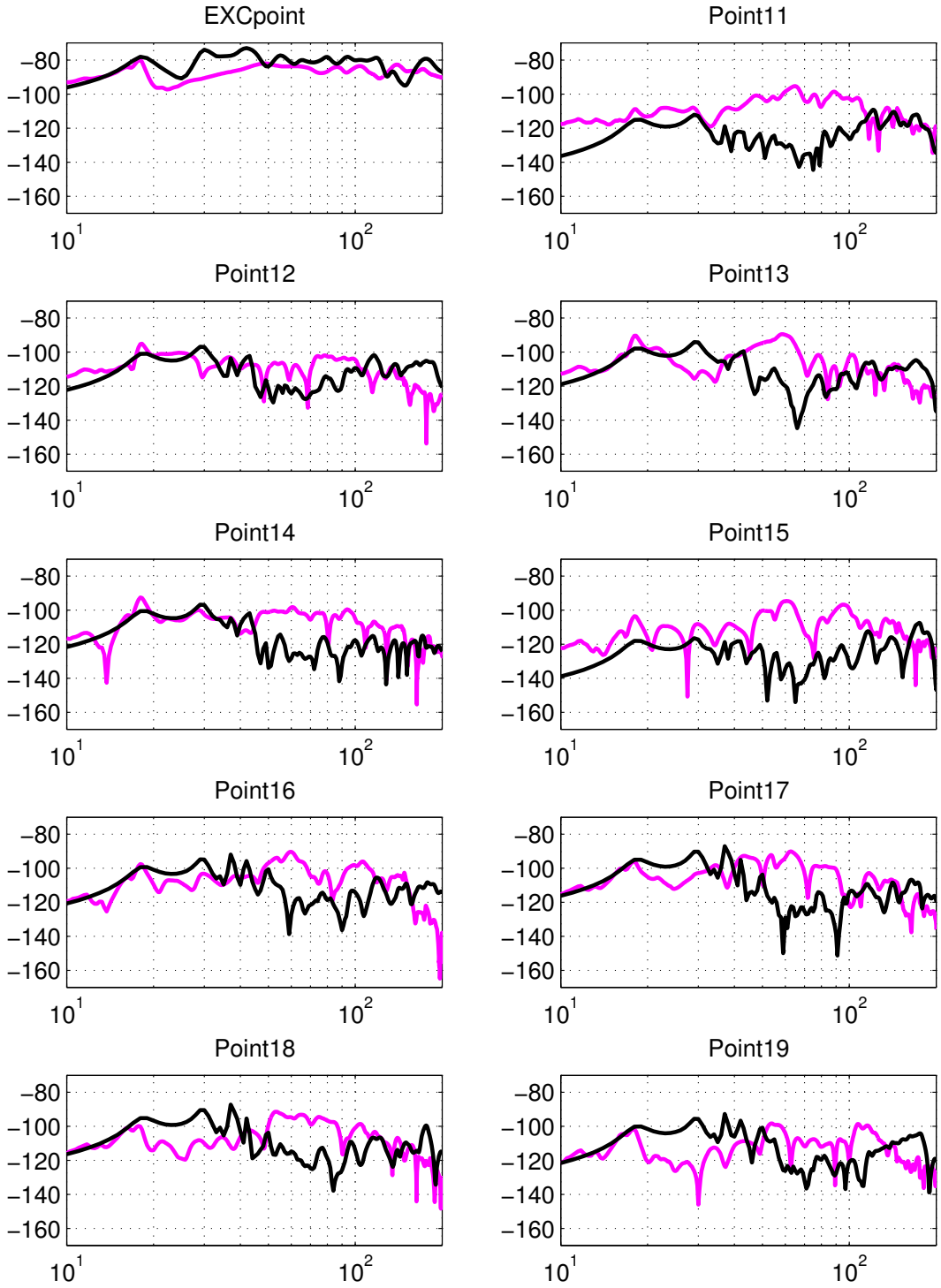

Figure 4.7.: Data comparison for points 11 to 19; thin purple lines for measured results and thick black for modeled by F.E.M. Mobility [dB ref. 1m/Ns] in vertical axis plotted over frequency [Hz, range; 10-200] in horizontal axis.

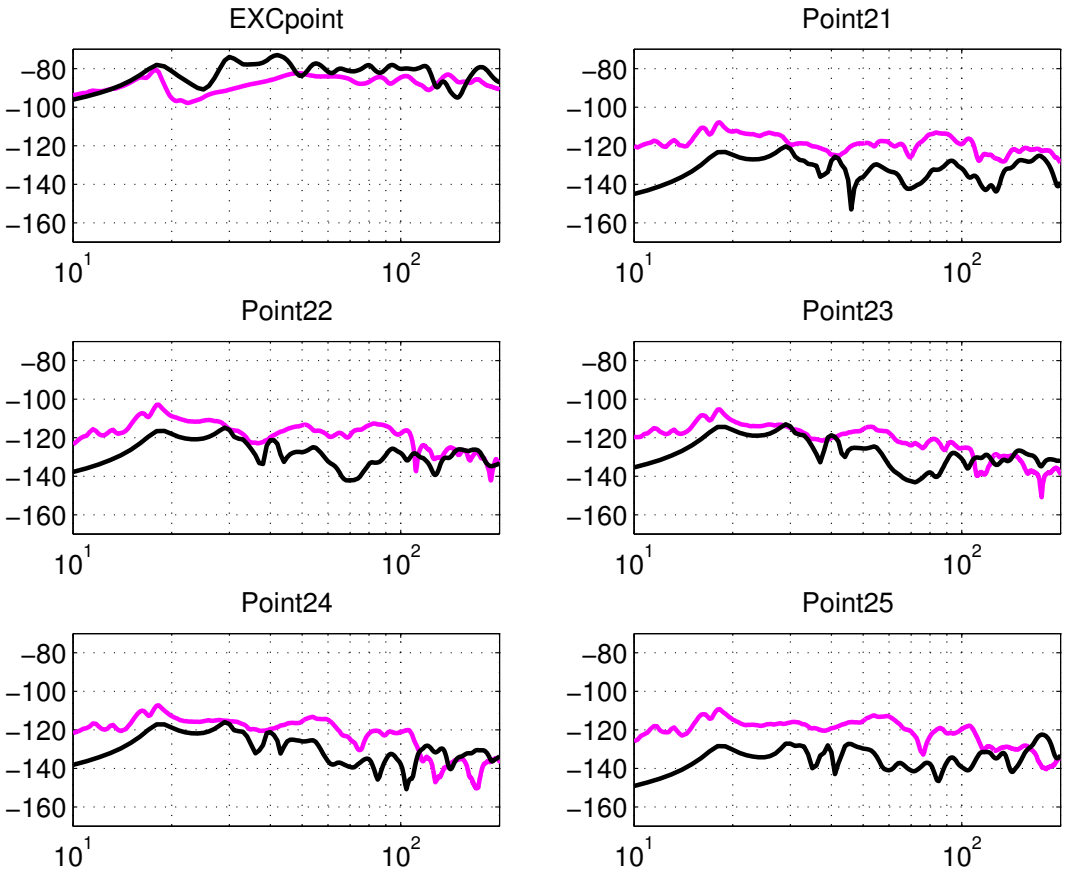

Figure 4.8.: Data comparison for points 21 to 25; thin purple lines for measured results and thick black for modeled by F.E.M. Mobility [dB ref. 1m/Ns] in vertical axis plotted over frequency [Hz, range; 10-200] in horizontal axis.

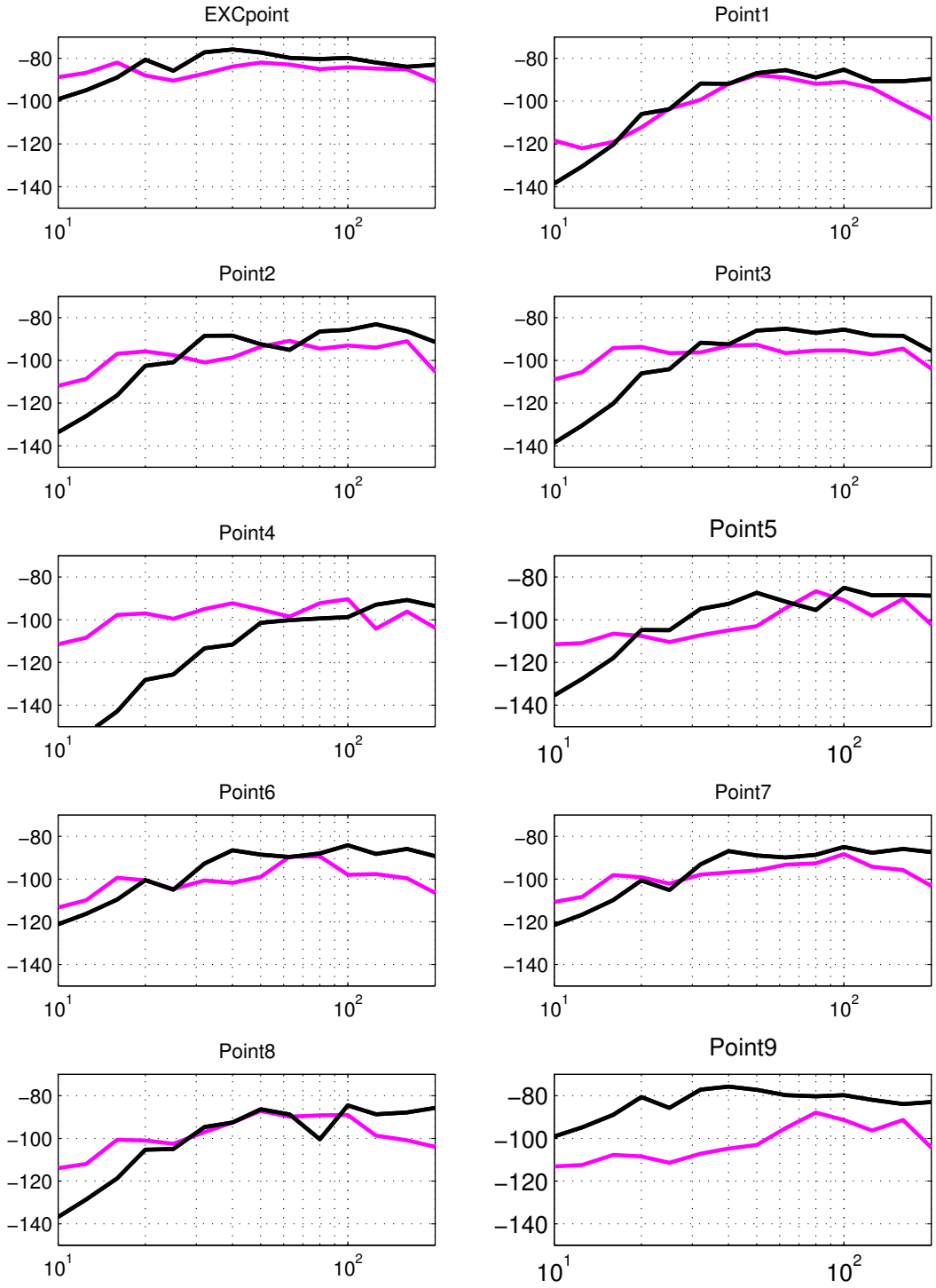

Figure 4.9.: Data comparison for points 1 to 9 in 1/3 octave bands; thin purple lines for measured results and thick black for modeled by F.E.M. Mobility [dB ref. 1m/Ns] in vertical axis plotted over frequency [Hz, range; 10-200] in horizontal axis.

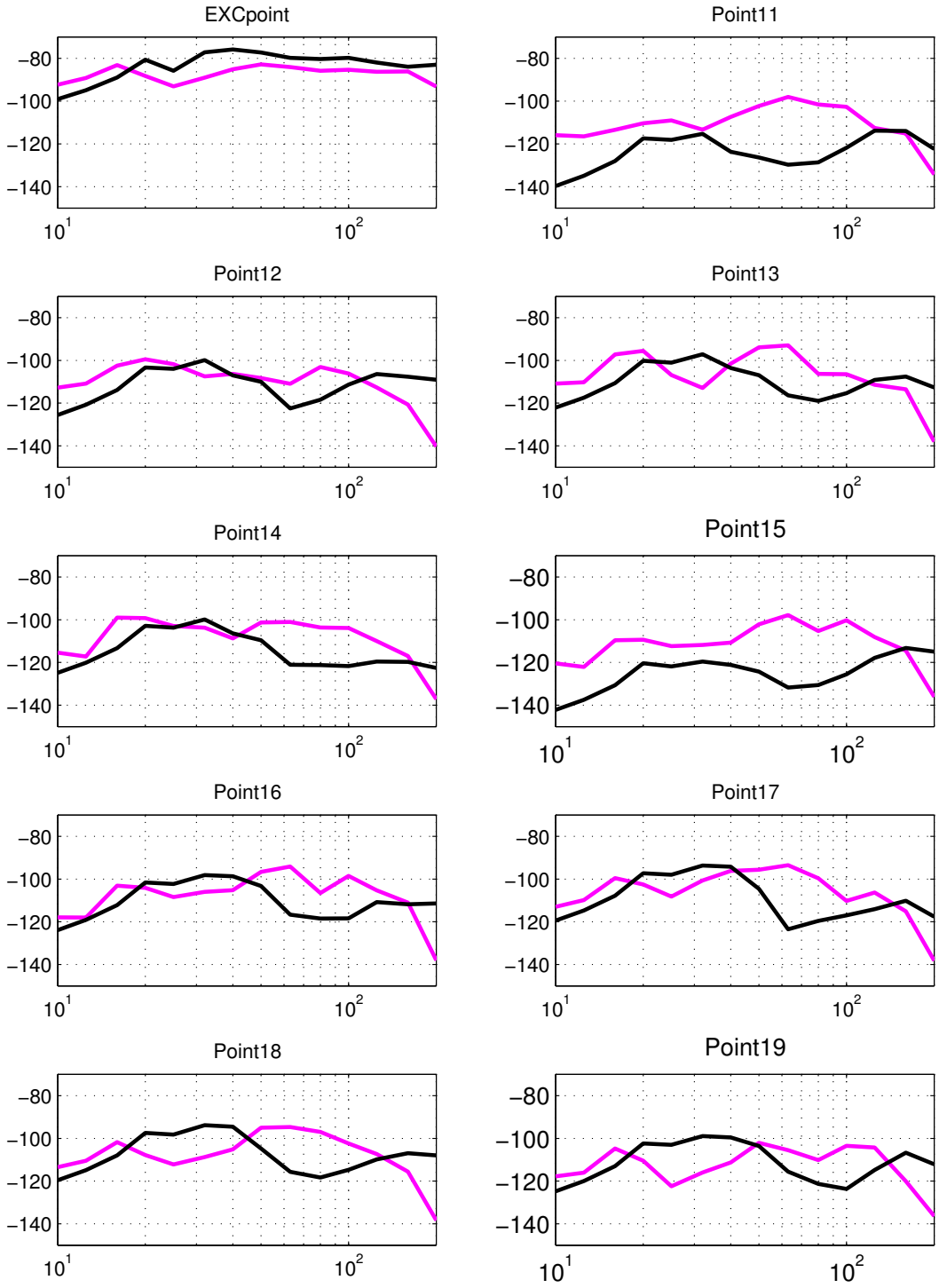

Figure 4.10.: Data comparison for points 11 to 19 in 1/3 octave bands; thin purple lines for measured results and thick black for modeled by F.E.M. Mobility [dB ref. 1m/Ns] in vertical axis plotted over frequency [Hz, range; 10-200] in horizontal axis.

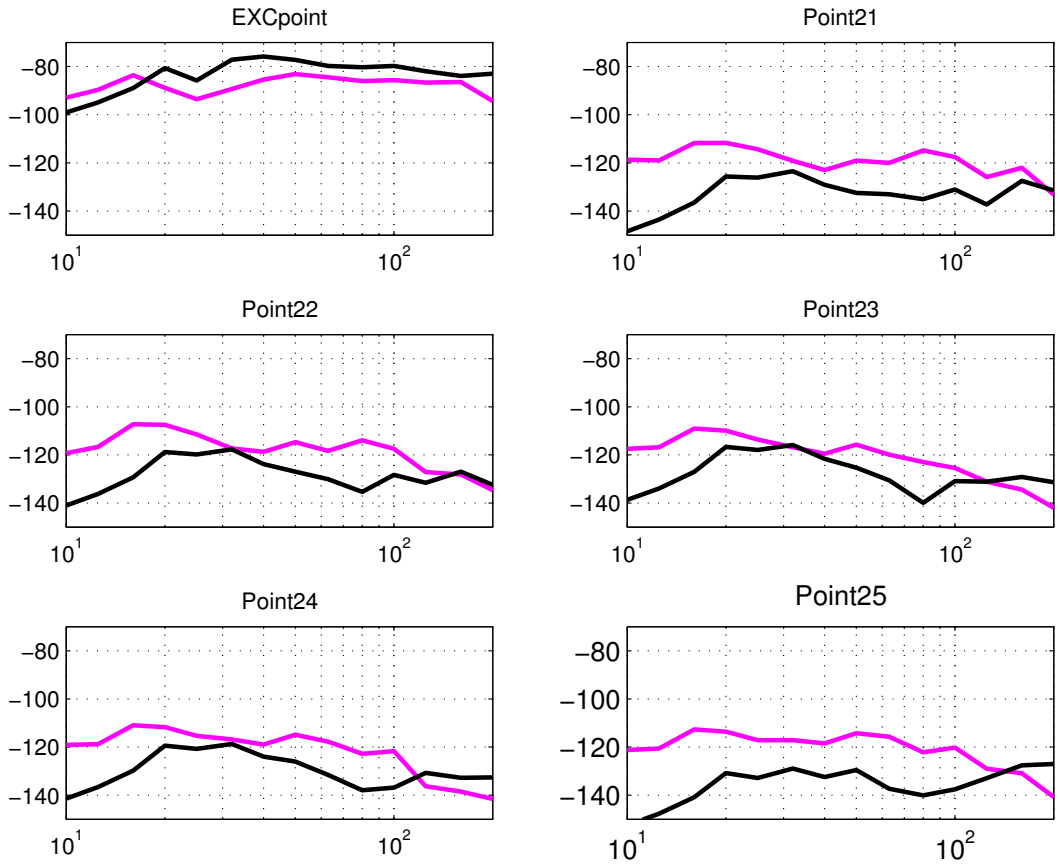

Figure 4.11.: Data comparison for points 21 to 25 in 1/3 octave bands; thin purple lines for measured results and thick black for modeled by F.E.M. Mobility [dB ref. 1m/Ns] in vertical axis plotted over frequency [Hz, range; 10-200] in horizontal axis.

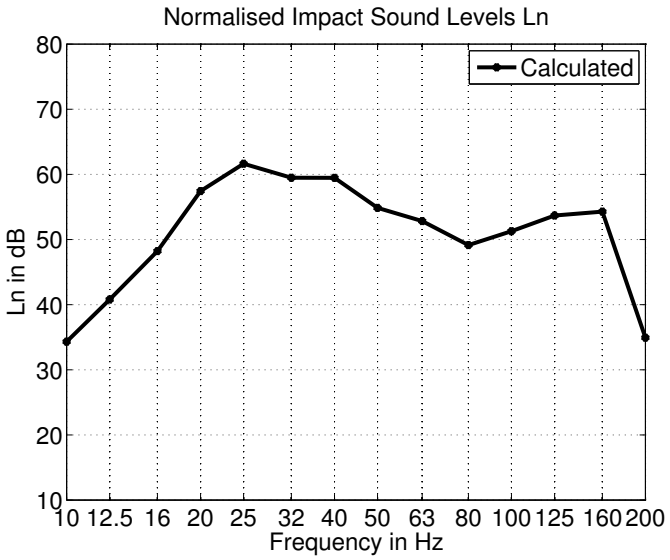

Figure 4.12.: Calculated results of Impact Noise Levels in 1/3 octave bands [dB ref. 2e-5 Pa] in vertical axis plotted over frequency [Hz, range; 10-200] in horizontal axis.

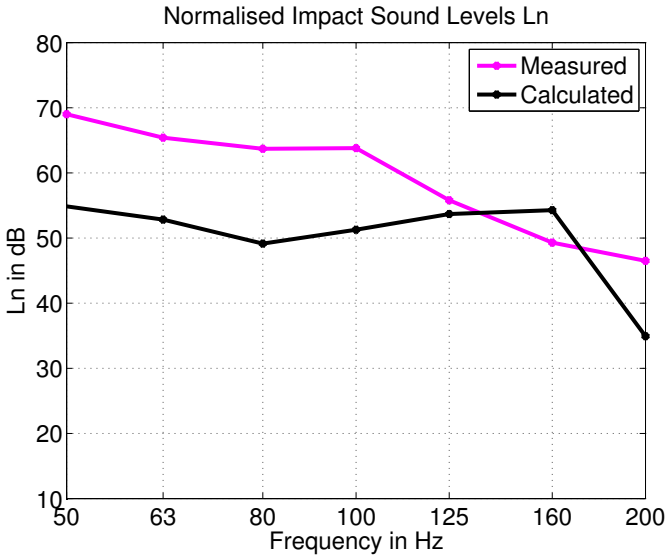

Figure 4.13.: Comparison of Impact Noise Levels in the room below the test floor structure in 1/3 octave bands; purple line for measured and black for calculated levels [dB ref. 2e-5 Pa] in vertical axis plotted over frequency [Hz, range; 50-200] in horizontal axis.

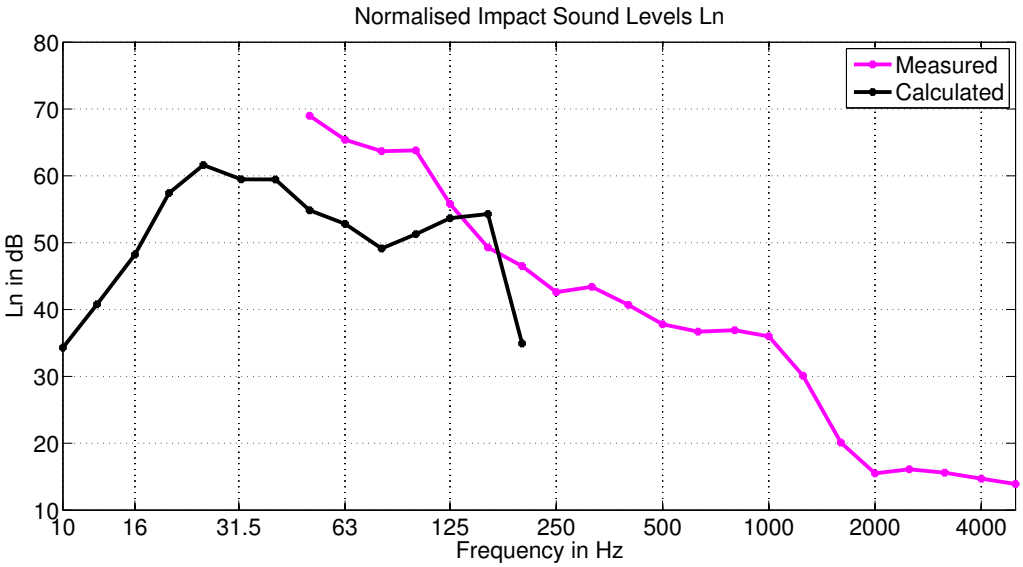

Figure 4.14.: Comparison of Impact Noise Levels in the room in 1/3 octave bands full results spectrum; purple line for measured and black for calculated levels [dB ref. 2e-5 Pa] in vertical axis plotted over frequency [Hz, range; 10-5000] in horizontal axis.

5. Discussion

5.1. Analysis of the measured results

The first conclusions about the test floor could be extracted directly from the measurements. The first mode of the structure is clearly excited at 18 Hz, as shown in all plots, having the maximum amplitude level of the curve at -80 dB. The next modes are not sufficiently visible in all plots, especially up to 100 Hz. Some of the basic resonances appear between 60 and 100 Hz in some plots but not clearly enough.

The general behavior of the structure seems to be very damped, as there are not any sharp resonances. Studying other mobility plots, like in Figure 2.3, it is apparent that non-damped resonances could be 10 to 20 dB higher than the case of our test structure. According to the half-bandwidth method, for the first resonance a loss factor of 0.085 could be calculated. However this is only an approximation.

Comparing the impact propagation from the excitation point to the transfer points the following conclusions can be made:

- There is at least 10 dB attenuation from the center of the slab to the edges, at the floor side (Points 1-9, Figures 4.1 and 4.2).

- Points 1, 5 and 9 have slightly lower response than the others, due to their position closer to the floor corners .They are more clamped and therefore heavier damped. Exactly the same happens also at the ceiling for transfer points 11, 15 and 19.

- The vibration transmission at the ceiling transfer points is reduced by circa 20 dB as a common trend for the low frequencies. Above 200 Hz the attenuation can reach up to 40 dB. The same situation exists for the flanking transmission measurement at the wall.

However, it should be mentioned that all transfer points in the results are close to the edges. That means that they are positioned in the stiffer areas of the structure and measurements in other surface points could show different mobility responses.

The coherence results for all measurements are illustrated in the Appendix chapter.

They are satisfactory (higher than 0.85) but only for the frequency range of interest. Directly above 200 Hz there are significant fluctuations or drops. This is expected as long as the impact hammer used offers efficient excitation below 500 Hz. Some occasional problems exist for the coherence in points 4, 5, 6, 8, 11 to 15, 18, 19 even below 200 Hz. However, the results could be generally and safely considered valid for the purposes of this study.

5.2. Comparison between F.E.M. results and measurements; mobility and impact noise levels

In Figures 4.6 to 4.11 the comparisons between the simulated and the measured results are presented for every individual transfer point and the driving point (denoted as EX-Cpoint). The frequency range of study for the comparison is 10-200 Hz. There is a degree of agreement between modeling and reality but also visible deviations which are expected and acceptable for the framework of this experimental study.

Specifically, a correlation for the first resonance was achieved. The same happens in many cases for the higher resonance frequencies and the anti-resonances of the system as well. The overall behavior of the mobility responses is approximated sufficiently but there are many inconsistencies either in amplitude levels or frequency positions.

For some points a slight shifting of the curve is noticeable but there is still a good agreement. In most results the problem is in the mobility levels which differ up to 40 dB in some cases. Usually the modeled results are significantly lower than the measurements, like for points 1, 11 and 21-25. In some other cases, especially for the transfer points 12-19 on the ceiling, the amplitudes coincide up to 50 Hz and then the F.E.M. curves drop down locally for 50-100 Hz. Finally, there are few cases, such as transfer points 18 or 19 where the simulated curve is partially up to 20 dB higher.

Additionally, the compared results of the excited floor have a significantly higher agreement than the ones on the ceiling or the wall below that. This is normal due to the closer distance and shorter transfer path, which is mostly affected by the same material, the concrete screed, and the same boundary conditions of that structural layer. The suspended ceiling is also connected with the floor through the CLT horizontal beams, the CLT plate and finally a thin aluminum grid (acoustic profile), which complicates the transfer path a lot for points 11-19.

In Figure 4.12, the impact noise levels are presented for the frequency range of study,

10 - 200 Hz. The calculation of that curve is based on the acquired results from the F.E. model. As can be seen, the impact noise levels of the room below the test floor are fluctuating between 40 and 60 dB especially for the frequency bands between 20 - 160 Hz. The levels are higher above 16 Hz where more structural modes exist and more energy is gathered in the frequency bands.

The differences between measured and calculated results are again visible as they reach up to 15 dB (Figures 4.13 and 4.14). However, considering the previous deviations observed in the mobility comparisons, these deviations in 1/3 octave band impact sound levels are normally expected. Consequently, the results are acceptable. They also indicate an amplitude drop in the frequencies below 50 Hz. The latter is significant because that low frequency behavior is not captured by ISO standard measurements (range: 50-5000 Hz) but it is the subject of interest in this study case.

5.3. F.E. model evaluation and limitations

The complexity level of the F.E. model is high and the important deviations need to be analyzed. Significant discrepancies in the resonance frequencies are usually existent in the outcome of the Finite Element analysis. This is the reason that material properties need to be tuned and simulations to run again until there is a satisfactory agreement with the measurements. Finally after tuning, the first modes can be calculated correctly as seen in the study case as well.

The most significant problems occur in the mobility levels where deviations could vary from 10 dB (acceptable for the scope of this thesis) up to 40 dB (not accepted). There are many reasons for those inaccuracies (the ones bigger than 10dB) which have to do mostly with the model setup, especially when the geometry is complex. Those complex cases demand simplified ways to represent the physical phenomena and boundary conditions, whereby many assumptions take place.

For this study implementation, the model includes 8 different materials for calculation and a multilayered structure, which makes it difficult to have better results than the ones acquired. The combination of those materials and their junctions make the transfer paths and the calculations very complex, raising the amount of inaccuracy.

Structural details, such as the aluminum grid of the acoustic insulation profiles and the wooden supporting beams connecting the chipboard to the CLT walls, can be tricky. Although they are included in the model there is no evidence that they interact correctly

in the dynamic simulation. Their dimensions are very small compared to the big volumes of CLT elements. It is also assumed that all layers form a union, meaning clamped connections at their boundaries, which does not correspond completely to the real case.

Furthermore, other parts of the structure like the metal connectors for the CLT parts, the glued layers, the screws and bolts are not included in the model due to their small size. However, those small parts play an important role in the transmission of vibrations between elements because they are rigidly connected. Even if they could be modeled as point boundaries, it is not known technically where they are placed within the slab. So they cannot be included in the F.E.M. design but they affect the real mobility response.

Concerning the calculation part of this study, there are sources of error that should be noted as well. Firstly, the values of material properties cannot be precise and they are usually given with some approximation in the literature. This level of deviation affects directly the simulations and their comparison to real measurements. Secondly, the tuning of material properties lead sometimes to unrealistic values that offer better results approximation, and thus be accepted.

In addition, the physical behavior of materials is also involved in assumptions, with linear and isotropic response being the most common. However, it is known that materials like CLT, with crosswise grain layers, are strongly anisotropic, i.e. they have different properties for each direction. Some properties are also frequency dependent in reality such as the loss factor and Young's modulus. However, constant values were used here, instead of matrices for different frequencies or directions, for convenience and simplicity in the simulations. All the above factors combined can affect the calculation process in many ways, which are not obvious. Hence, the sources of uncertainty cannot be easily identified.

6. Conclusions

The applications of F.E. models in research or industry can be a useful engineering tool. The main reason for this experimental study as well was to develop a sequence of calculations with Finite Element Method that would be considered valid. This was achieved up to a point but serious errors and deviations from reality were found as well. Thus the results of the study cannot be considered professionally good but they remain acceptable and useful within the limitations of this thesis.

The acquired results concerning amplitude levels and frequency position are strange in same cases. That makes some transfer point results not valid for comparisons and they should be neglected. However, differences in levels around 10 dB can be considered acceptable for this study case and they offer valuable information for the investigation of the structure.

Generally, the mobility plots in 1/3 octave bands show a significantly better agreement between measured and modeled results (due to averaging within the bands) than the narrow band comparison.

The calculation of impact noise levels offered satisfactory results for this case, considering the bigger deviations in the mobility graphs. However, this process remains a numerical approximation with large uncertainties.

Little experience exists about modeling complicated structure types. The sources of possible error are numerous and the development of such a F.E. model relies on the researcher, including assumptions, changes and simplifications.

Summing up, the deviation between modeling and reality is always existent. In the study case of this thesis, a model of a multilayered structure with complex joints was set up, calculated and evaluated. The outcome is positive for an experimental study like this, although the analyzed calculations could not be used as a professional tool yet. However better results can be possible with further investigation and with developing the individual parts of the process before combining them in complex F.E. modeling. Specific suggestions for research continuation are analyzed in the next chapter.

7. Future work suggestions

For acquiring better and solider results in the future, additional studies need to be done and deeper experience to be gained. Some suggestions for continuation of the studies are;

- Combination of F.E.M. and B.E.M. (Boundary Element Method) modules for calculations of sound field pressures in adjacent rooms. Then, those results can be compared with Airborne and Impact Sound ISO measurements or narrow band FRFs of sound pressure levels. Another way for this application would be to model the air as a volume in F.E.M. using appropriate parameters and acquire velocities to approximate pressure levels.

- Specific measurements for every material to define the properties more accurately. Use of frequency dependent values for elasticity modulus and loss factor would capture the behaviour of materials properly. After approximating the properties of the materials individually, complex Finite Element modeling could be done with less error possibilities. Establishing limits for tuned parameters is also important.

- Further study of CLT as a material with focus on its anisotropic behaviour. The use of Young's modulus matrices for different directions and testing in F.E. modeling needs to be developed.

- Thorough investigation of modeling complex structures with more than 3 materials. Acceptable deviation limits between measurements and real results need to be used.

- Continuation of measurements in lightweight structures and comparison with modeled results. Lab measurements of structural junctions of various types would be also useful for the study of CLT structures.

- Further study on the appropriate theory for dynamic behaviur using analytical solutions. Comparison of outcomes from different software could be done to compare the performance of F.E.M. approaches.

Bibliography

[1] J. Brunskog S. Ljunggren D. Bard G. Sandberg F. Ljunggren A. Ågren O. Hallström H. Dybro K. Larsson K. Tillberg L-G. Sjökvist B. Östman K. Hagberg Å. Bolmsvik A. Olsson C-G. Ekstrand M. Johansson J. Forssén, W. Kropp. *Acoustics in wooden buildings. State of art 2008*. SP Sveriges Tekniska Forskninginstitut, 2008.

[2] J. Negreira. *Vibrations in Lightweight Buildings - Perception and Prediction*. Lund University. Department of construction science., http://lup.lub.lu.se/record/4090700, 2013.

[3] K. Hagberg. *Design of lightweight constructions - risks and opportunities*. Internoise, 2009.

[4] *Acuwood Research Programme*. www.acuwood.com.

[5] K. Hagberg C. Simmons, F. Ljunggren. *Findings from the AkuLite project: New single numbers for impact sound 20-5000 Hz based on field measurements and occupants' surveys*. Internoise 2013 Innsbruck.

[6] *Woodwisdom-net*. www.woodwisdom.net.

[7] *Fristadsbygg*. www.fristadbygg.se.

[8] *WSP Group Environmental*. www.wspgroup.com/sv/wsp-sverige/.

[9] *Building Physics*. KLH Massivholz GmbH, www.klh.at, 2012.

[10] *Introduction to COMSOL Multiphysics*. www.comsol.com/shared/downloads/IntroductionToCOMSOLMultiphysics.pdf, 2013.

[11] H. Kuttruff. *Acoustics: An Introduction*. Taylor & Francis, 2007.

[12] M. Kleiner. *Acoustics and Audio Technology*. A Title in J. Ross Publishing's Acoustics: Information and Communication. J. Ross Pub., 2011.

[13] B.A.T. Petersson L.Cremer, M.Heckl. *Structure-Borne Sound: Structural Vibrations and Sound Radiation at Audio Frequencies*. Springer, 2005.

[14] W.Kropp. *Technical Acoustics*. Chalmers University of Technology, Gothnburg, Sweden, 2007.

[15] T.E. Vigran. *Building Acoustics*. Taylor & Francis Group, 2008.

[16] *Structural Mechanics Module User's Guide*. COMSOL, 2012.

[17] *Finite Element Models applied in Active Structural Acoustic Control*. M.H.H. Oude Nijhuis, A. de Boer, 2002.

[18] K. H. Heron F. G. Leppington, E. G. Broadbent. *The Acoustic Radiation Efficiency of Rectangular Panels*. Proceedings of the Royal Society of London. 1982.

[19] *National Instruments Modal View Software*. http://sine.ni.com/nips/cds/view/p/lang/sv/nid/210054.

[20] A. Sjöström J. Negreira and D. Bard. *Investigation of the Vibration Transmission Through a Lightweight Junction With Elastic Layer Using the Finite Element Method*. Inter-Noise 2012, New York, USA.

[21] *MATLAB Simulink R2012b*. Mathworks, http://www.mathworks.se/.

[22] *EN12354-2 Building acoustics - Estimation of acoustic performance in buildings from the performance of elements - Part 2: Impact sound insulation between rooms*. European Committee for Standardization.

[23] *ISO 140-7:1998 Acoustics – Measurement of sound insulation in buildings and of building elements – Part 7: Field measurements of impact sound insulation of floors*. ISO (International Organization for Standardization).

[24] *ISO 717-2:2013 Acoustics – Rating of sound insulation in buildings and of building elements – Part 2: Impact sound insulation*. ISO (International Organization for Standardization).

A. Appendix

This section includes additional material of the study , which did not need to be in the text, for ease of reading. In the following pages can be found: construction details of the building, photos of every measurement part (sets of 5 measurement points), pictures of vibrational patterns from the F.E. model and the coherence plots.

Figure A.1.: Photo of the building during construction. Details of parts that are covered behind the gypsum walls at completion can be seen.

Figure A.2.: Photo of the measurement set at points 1-5 on the floor.

Figure A.3.: Photo of the measurement set at points 5-9 on the floor.

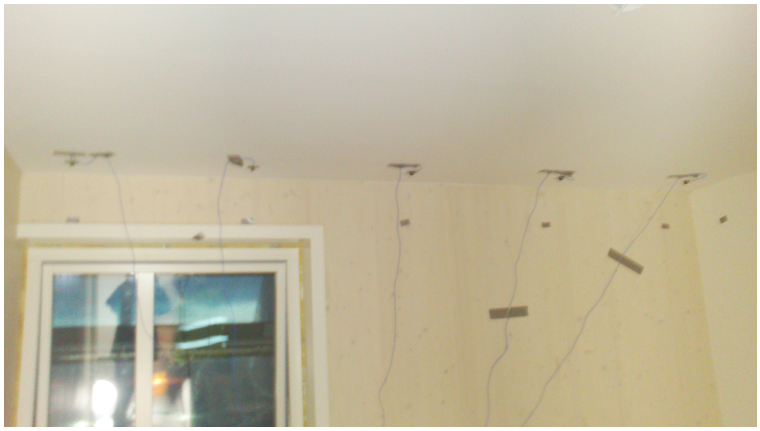

Figure A.4.: Photo of the measurement set at points 11-15 at the ceiling.

Figure A.5.: Photo of the measurement set at points 15-19 at the ceiling.

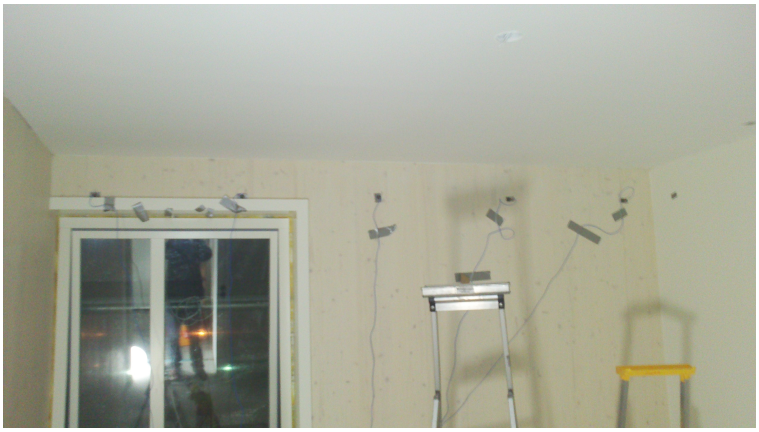

Figure A.6.: Photo of the measurement set at points 21-25 at the wall.

Figure A.7.: Photo of the measurement set at points 26-30 at the wall.

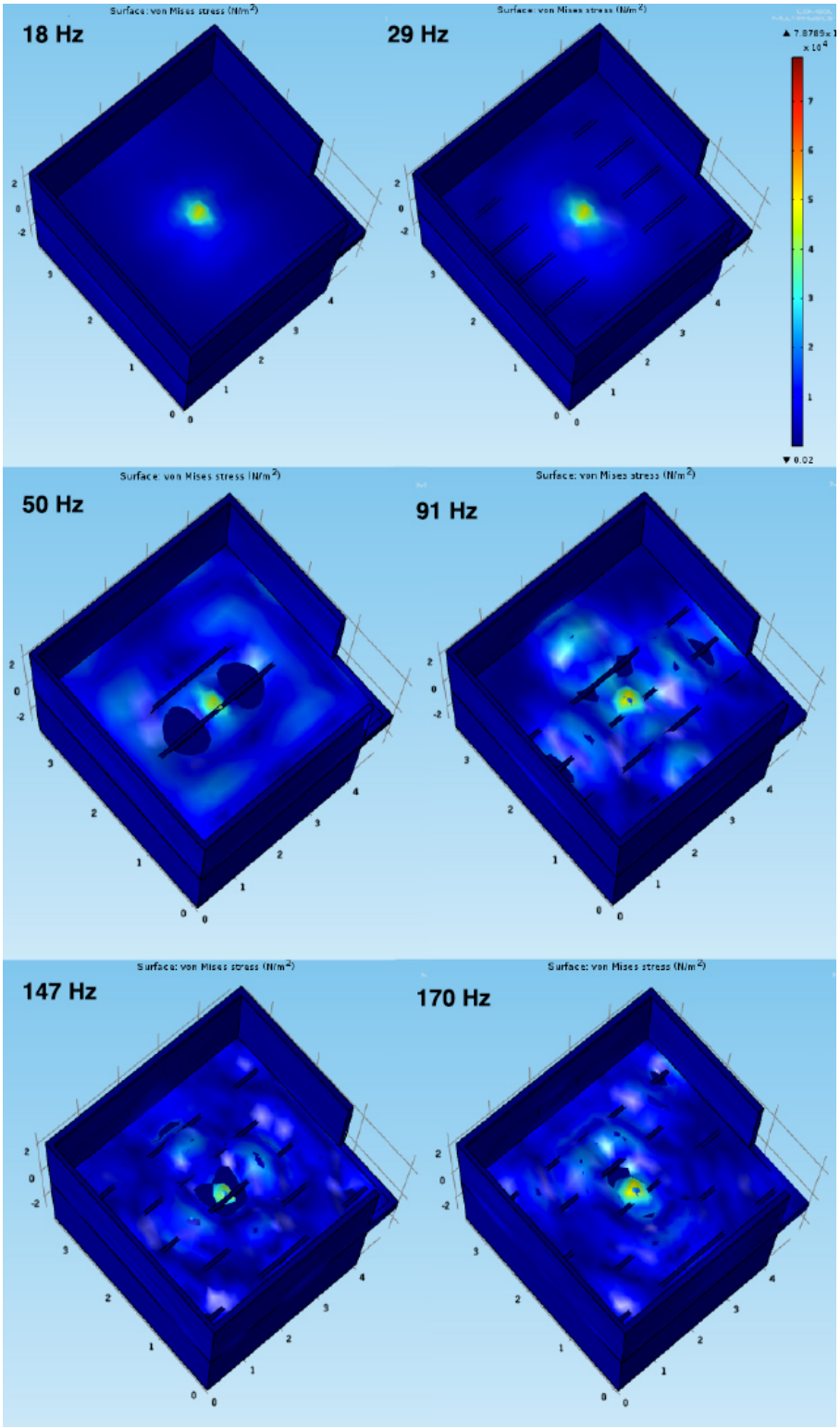

Figure A.8.: Image presenting visually some representative vibration patterns (modal shapes) of the test structure as acquired by the Finite Element model.

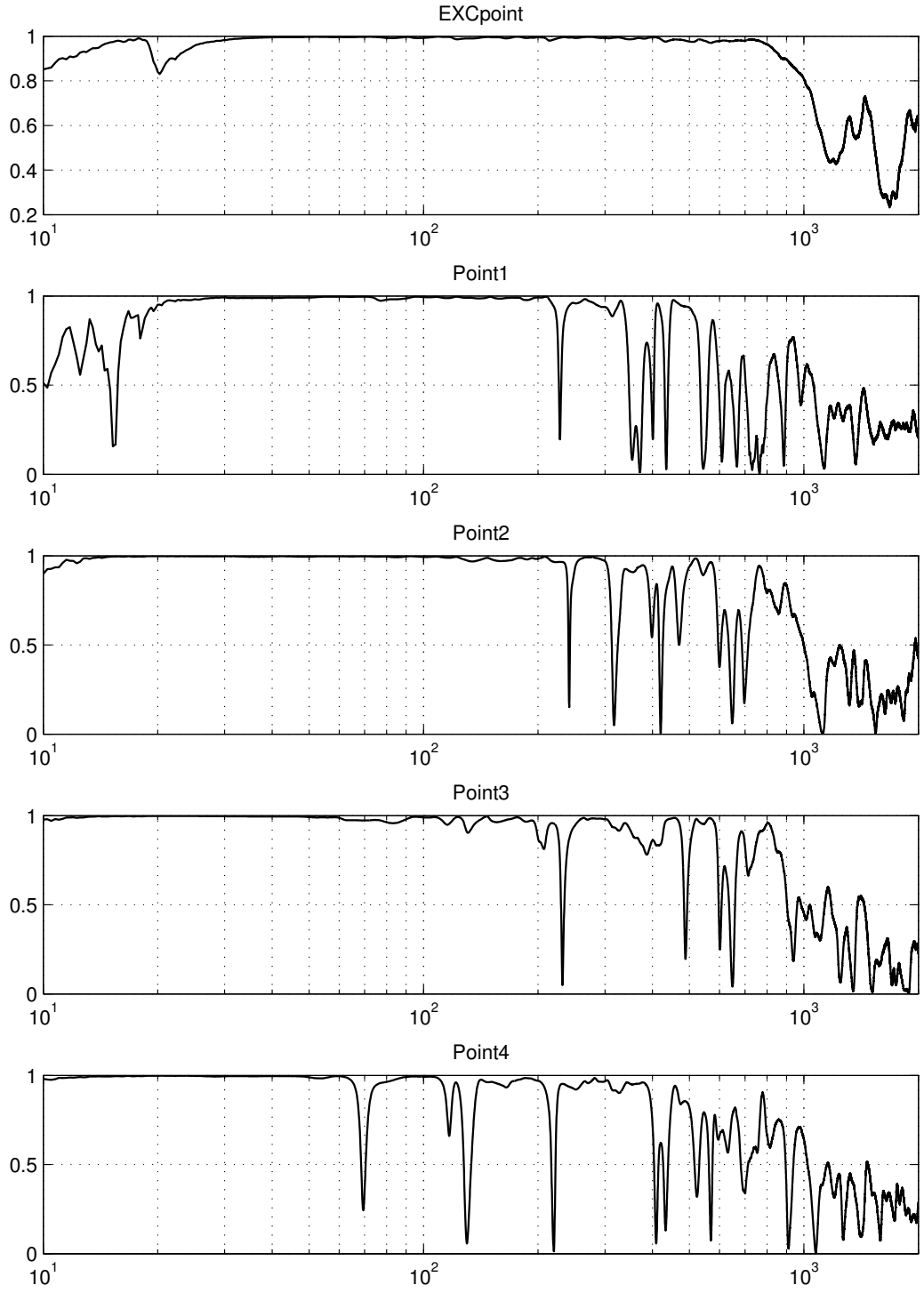

Figure A.9.: Measurements of the construction; driving point (EXC) and transfer points 1 to 4. Coherence in vertical axis plotted over frequency [Hz, range; 10-2000] in horizontal axis.

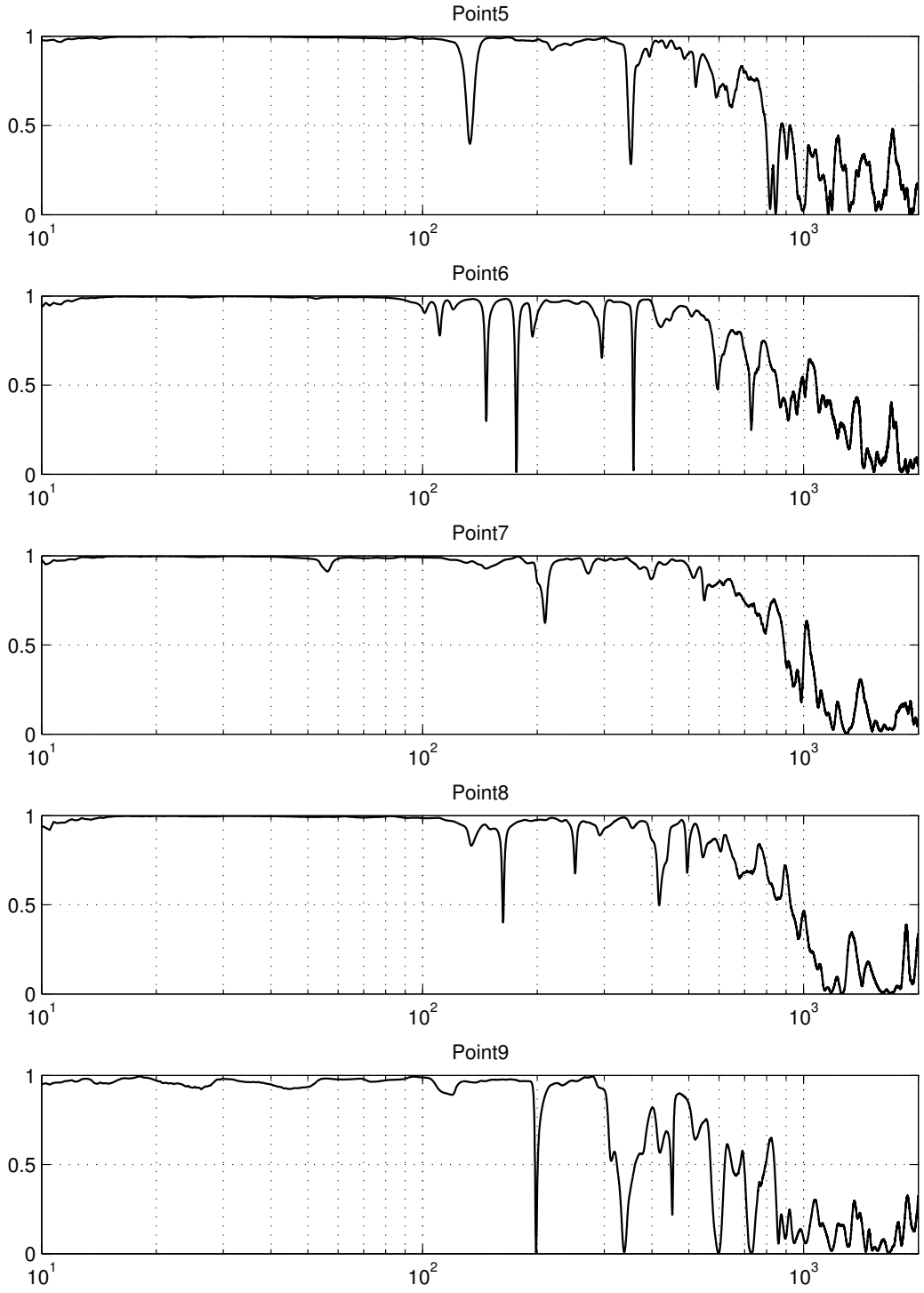

Figure A.10.: Measurements of the construction; transfer points 5 to 9. Coherence in vertical axis plotted over frequency [Hz, range; 10-2000] in horizontal axis.

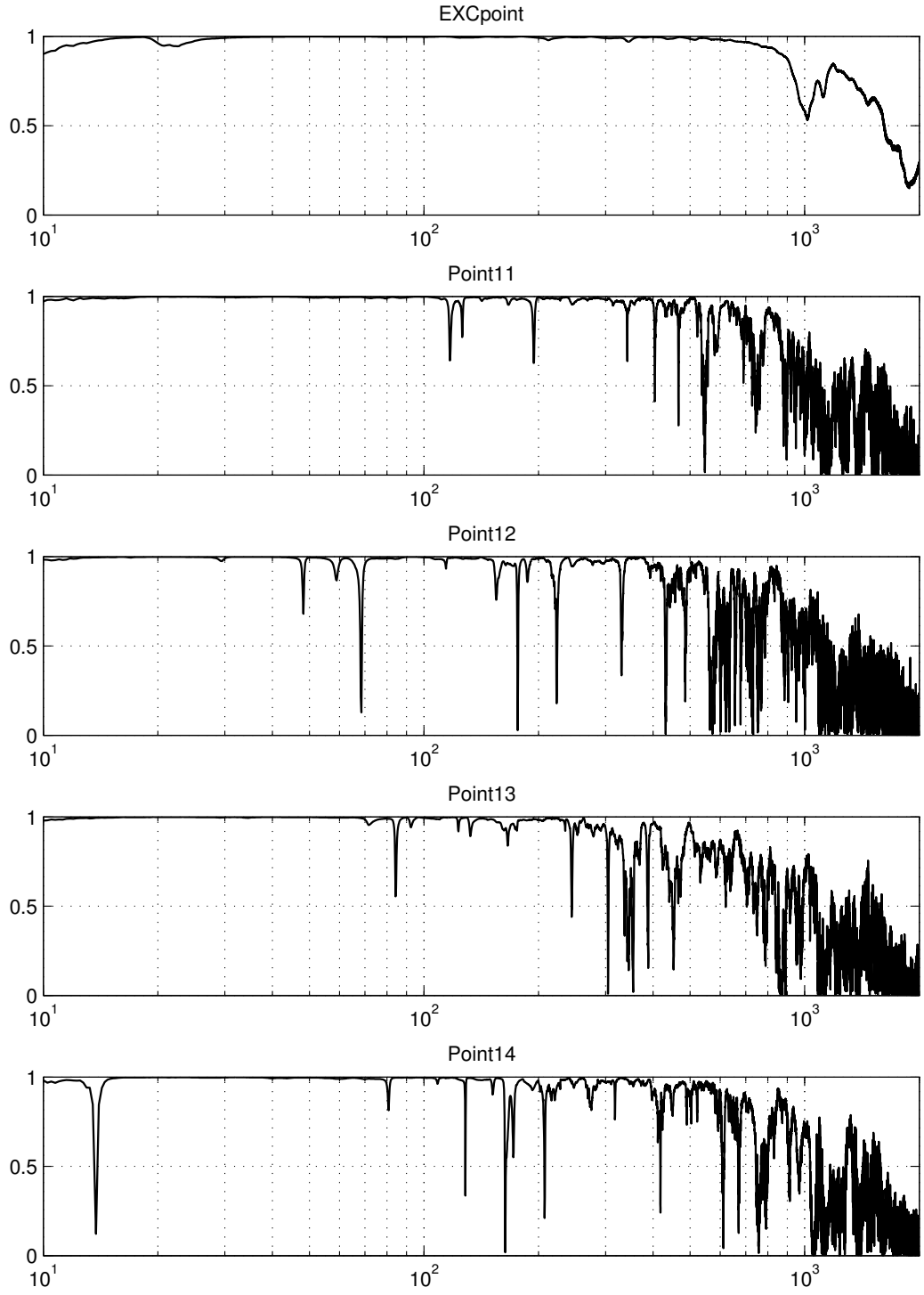

Figure A.11.: Measurements of the construction; driving point (EXC) and transfer points 11 to 14. Coherence in vertical axis plotted over frequency [Hz, range; 10-2000] in horizontal axis.

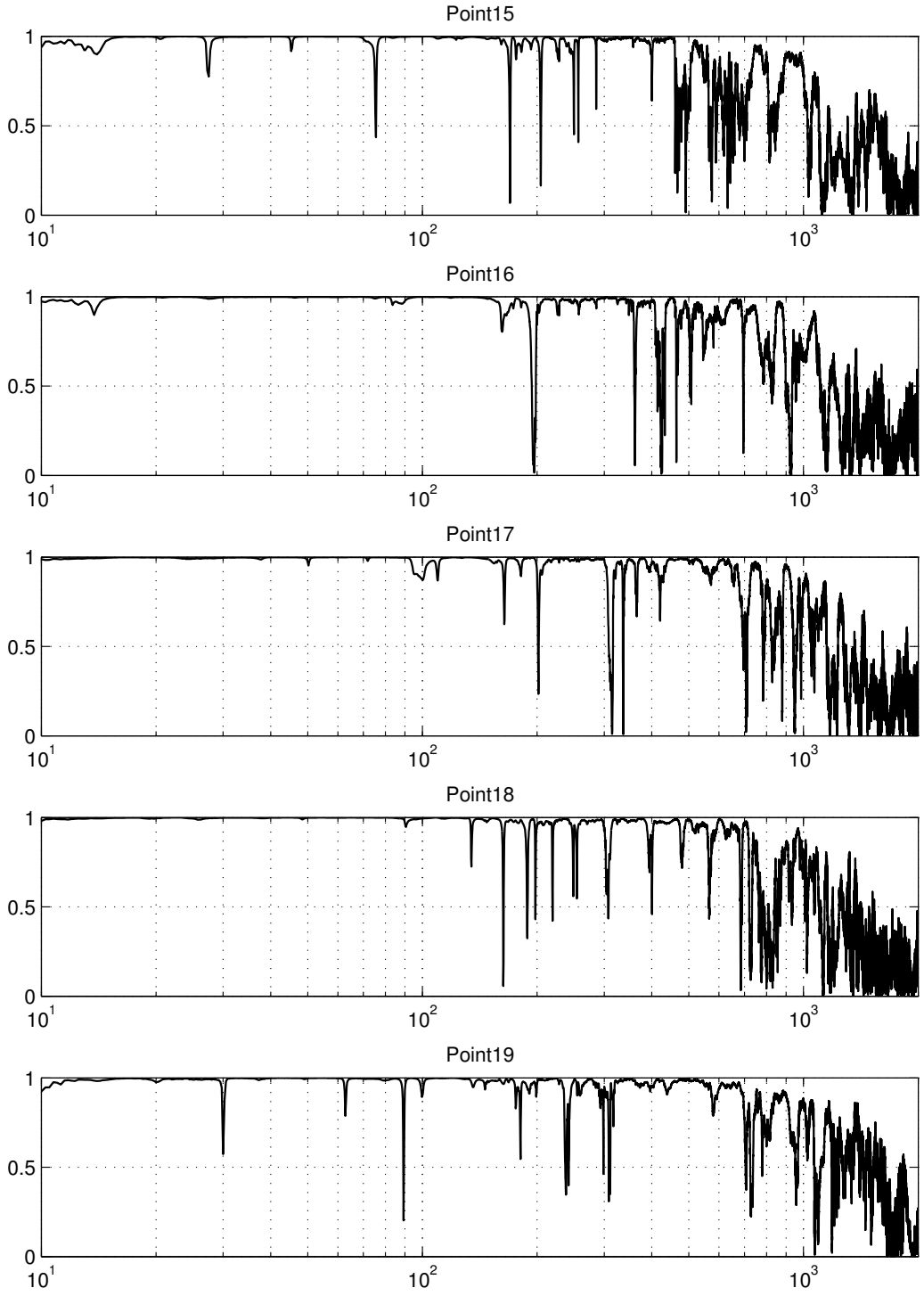

Figure A.12.: Measurements of the construction; transfer points 15 to 19. Coherence in vertical axis plotted over frequency [Hz, range; 10-2000] in horizontal axis.

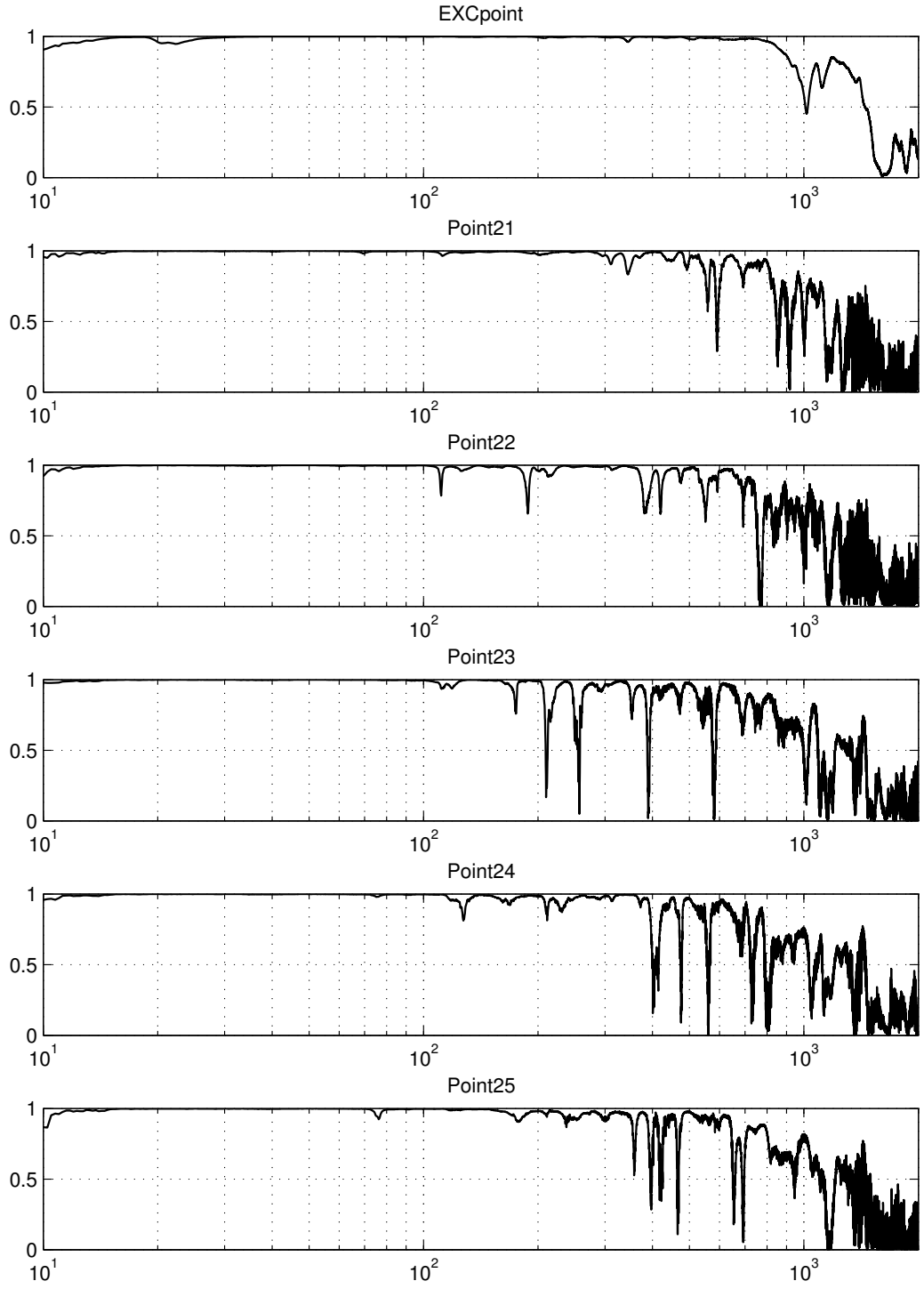

Figure A.13.: Measurements of the construction; driving point (EXC) and transfer points 21 to 25. Coherence in vertical axis plotted over frequency [Hz, range; 10-2000] in horizontal axis.